Journal of Building Engineering 114 (2025) 114112

Contents lists available at ScienceDirect

Journal of Building Engineering

journal homepage: www.elsevier.com/locate/jobe

On the use of recycled UHPC to reduce cement demand in UHPC mixes: mechanical and durability validation

Marco Davolio [a,*], Estefania Cuenca [a], Davide di Summa [a], Ruben Paul Borg [b], Liberato Ferrara [a]

[a] Department of Civil and Environmental Engineering, Politecnico di Milano, Piazza Leonardo da Vinci 32, 20133, Milan, Italy
[b] Faculty for the Built Environment, University of Malta, Tal-Qroqq, Msida, MSD 2080, Malta

ARTICLE INFO

Keywords:
UHPC
Recycling
Self-healing
LCA
Sustainability

ABSTRACT

Ultra-High Performance Concrete (UHPC) offers superior durability and strength, as compared to ordinary concrete solutions, but its inborn environmental footprint is dictated by high cement content and the environmental impact of raw material extraction, which would require a heavily optimized structural and process design to be levelled off. With the aim of assessing effectiveness of strategies aimed at reducing the embodied carbon footprint of UHPC mixes, this study investigates two recycled UHPCs (R-UHPC) designed by replacing all natural aggregates with crushed UHPC and partially substituting Portland cement (30 %) with recycled material. One mix used ungraded crushed UHPC; the other included additional fine fractions (≤75 μm) obtained through further processing. The partial replacement of cement constitutes a novelty alongside the widely established aggregate replacement in high performance cementitious materials. Both mixes achieved superior compressive strength and comparable flexural strength to the reference UHPC, while demonstrating effective autogenous self-healing under repeated NaCl exposure, with full recovery of crack sealing, sorptivity, strength, and stiffness over six months. However, the mix containing recycled fines showed reduced performance under repeated damage-healing cycles, mainly attributed to its higher water absorption. A cradle-to-gate life cycle assessment using the CML-IA method and a functional unit of 1 m^3 – subsequently normalized over long-term compressive and flexural strength – revealed that mechanical performance strongly influences environmental impacts. Notably, the additional processing and increased input volumes required for fine fractions led to higher impacts across all categories. This work lays the foundation for a rational and engineering-wise effective promotion of the circular economy concept in the design and production of highly durable cement-based materials and structures by demonstrating unexplored and effective recycling strategies for UHPC elements at the end of their service life, facilitated by their unaltered condition even after prolonged use.

1. Introduction

The environmental impact of concrete production, particularly due to cement, presents major challenges for the construction industry in its pursuit of sustainability. With global Portland cement consumption at 4.1 billion tonnes [1], this demand is expected to

* Corresponding author.
E-mail address: marco.davolio@polimi.it (M. Davolio).

https://doi.org/10.1016/j.jobe.2025.114112
Received 19 May 2025; Received in revised form 29 August 2025; Accepted 16 September 2025
Available online 10 October 2025

grow further as infrastructure development accelerates worldwide. In addition to CO_2 emissions, the industry's demand for raw materials, including sand and gravel, raises concerns over resource depletion and habitat destruction. In 2023, the U.S. alone extracted 920 million tonnes of construction sand and gravel, 43 % of which was used for concrete [1]. The extraction and processing of these materials contribute to environmental degradation, while the waste generation by the construction sector also poses challenges for disposal and recycling [2]. A significant portion of this waste consists of construction and demolition waste (CDW), a mix of concrete, steel, glass, and hazardous substances, including, e.g., asbestos and mercury [3].

The need to mitigate the environmental impact of concrete production and address the challenges of waste generation has led to a growing focus on effectively implementing circular economy principles within the construction industry, aiming at closing material loops, reducing raw material consumption, and enhancing resource efficiency through the recovery, reuse and recycling of materials. One promising approach is the use of recycled aggregates (RA) derived from CDW to replace natural aggregates in concrete production. This strategy aligns with European Union Directive 2008/98/EC [4], which already set a target of 70 % recovery of non-hazardous CDW by 2020. As of 2022, the current state of waste recovery stood at 61.4 % (source: Eurostat), highlighting progress yet underscoring the need for continued efforts to meet and exceed this target. The adoption of recycled aggregates has gained momentum in recent decades, with research demonstrating its potential to reduce the environmental burdens of concrete production [5]. Studies indicate that concrete containing recycled aggregates can achieve comparable strength and durability to conventional concrete, depending on the source and quality of the recycled materials [6]. However, the use of recycled aggregates introduces variability in concrete properties, with potential impacts on mechanical strength [7], stiffness [8], and water absorption [9]. These drawbacks have been thoroughly examined by researchers, who have proposed mitigation strategies including surface treatments [10,11] and enforced carbonation [12], which can help mitigate their impact.

The development of Ultra-High Performance Concrete (UHPC) offers a pathway to address both durability concerns and resource efficiency [13], supporting the goals of sustainable construction. Its innovative design aligns with the United Nations Sustainable Development Goals (SDGs) – particularly Goals 9 (Industry, Innovation and Infrastructure), 11 (Sustainable Cities and Communities), and 12 (Responsible Consumption and Production). UHPC is characterized by a dense matrix, high strength, and enhanced durability [14,15]. Its composition includes finely graded aggregates, fibres for reinforcement, and a low water-to-binder ratio, resulting in reduced porosity and superior performance, even in aggressive environments [16]. This makes UHPC an attractive option for infrastructure exposed to harsh conditions, such as marine environments [17,18]. One of the key advantages of UHPC, which is often not properly valorised when compared, e.g., to its high compressive strength, is its signature tensile behaviour. Thanks to the stress redistribution capacity provided by the fibres crossing a cracked cross section, after first cracking and under increasing stress UHPC forms stable multiple micro-cracks rather than localizing the damage into the first single large crack, also resulting in strain hardening behaviour [19]. This multiple-cracking behaviour enhances the material's autogenous self-healing potential, whereby unreacted binder particles in the matrix hydrate over time to seal micro-cracks [20,21]. Considering that UHPC structures are also likely to work under cracked structural service scenarios, the aforesaid self-healing capacity can significantly extend the maintenance-free lifespan of UHPC structures, thus resulting in reduced costs and environmental impacts associated with maintenance repairs and replacements [22]. Beyond material optimization, structural efficiency can be achieved through design innovations that exploit UHPC capabilities [23,24], resulting in significant material savings already at the time of construction. This overall aligns with the broader goal of carbon-neutral structures, which aim to minimize both initial construction emissions and emissions throughout the structure's life cycle.

The production of Ultra-High Performance Concrete, however, poses significant challenges related to the embodied carbon of the most commonly adopted mixes, mainly due to the higher binder content. Although the remarkable structural efficiency of these materials allows for an overall reduction of the environmental impact of the structure if compared, for instance, to ordinary reinforced concrete structures, recent efforts tried to promote the sustainability of UHPC production. Various solutions have been investigated under the concept of sustainable or "eco-friendly" UHPC. As summarized by Lande and Thorstensen [25], a multifaceted strategy is required for the deployment of environmentally efficient UHPC, which should include, among other options, circularity, intended as utilization of by-products. The inclusion of solid waste, for instance, provides a portfolio of solutions, significantly abating the environmental footprint while preserving the peculiar features of UHPC [26], with detailed examples including the use of biomass ash as a pozzolanic binder [27] and biochar for the development of multifunctional cementitious composites [28]. Alternatively, recycling of existing structures can be a valuable option where the supply chain for other wastes would imply long transportation distances. For instance, Kannikachalam et al. [29] proposed a case-study where the existing UHPC structure terminates its service life, and a similar one must be built in the same location. The possibility of exploiting local recycling processes is a viable alternative to other sustainable mix designs, and it must be further investigated.

The implementation of circular economy concepts in the production of UHPC is relatively new, driven by its increasing use in bridge construction, repair projects, and other case-specific applications [30–32]. Currently, most studies have drawn on the extensive knowledge of recycled aggregate concrete (RAC) to incorporate recycled aggregates and fines into UHPC mixes with a reduced embodied carbon footprint. For instance, Chen et al. [33] and Li et al. [34] explored the use of recycled fine aggregates in UHPC, respectively focusing on the durability and mechanical properties of the mix. The implementation of recycled fines led to more pronounced multiple-cracking pattern and strain-hardening response, while preserving the compressive and tensile strength of the original mix. Moreover, flexural and tensile strength can be improved when high-quality aggregates are used in place of natural sand, as observed by Luo et al. [35,36], who treated the recycled materials to compensate for the poor physical properties of the as-received waste. Similarly, carbonation of recycled fines for the subsequent use in UHPC can slightly enhance the compressive strength for limited replacement ratios, up to 50 % [37]. On the other hand, durability properties such as capillary absorption and freeze-thaw resistance can be negatively affected by the utilization of recycled fines, possibly due to the reduced $Ca(OH)_2$ concentration, which

leads to fast surface carbonation [38,39].

However, using UHPC as a parent mix is rather unexplored, mainly due to its limited availability compared to ordinary concrete, particularly for structures at the end of their service life. Moreover, the recycling process for higher-grade concretes involves significant additional energy demand for the crushing, which must be offset by substantial reductions in the embodied carbon of the resulting recycled UHPC mix. As such, recycled aggregates and fines should not only replace natural sand but also partially substitute cement in new UHPC mixes, further reducing the embodied carbon of R-UHPC. This is feasible due to the substantial presence of unreacted binder particles [40], which can contribute to the hydration process in new mixes, thereby reducing the need for virgin cement. An attempt was made by Qian et al. [41] in partially replacing binder with dehydrated cementitious powder (DCP), obtained by treating recycled cementitious material. Albeit preserving the properties of the native mix, the use of DCP had a rather small impact on the environmental footprint due to the emissions associated to waste processing. Moreover, preserving the material's self-healing capability – a crucial factor for long-term performance in aggressive environments – remains a significant challenge. Medjigbodo et al. [42] thoroughly assessed the self-healing capability of a normal grade concrete mix with partial and total replacement of sand and gravel. According to the results described, the use of recycled aggregates has limited influence on self-healing kinetics of small cracks.

This work serves a dual purpose: first, to investigate the feasibility of re-using all the sizes of the constituents resulting from UHPC recycling. In fact, these processes imply that, alongside separated steel fibres, significant quantities of fines accumulate at each crushing step. Therefore, the possibility of replacing cement and aggregates with increased fines content would opportunistically align with the distribution of fractions of the recycled material. Second, this work aims to assess whether recycled UHPC mixes can retain their self-healing capabilities despite substituting virgin cement with recycled material, a key factor for maximizing the life-cycle benefits of the investigated category of materials in structural design.

To achieve these objectives, the mechanical performance of three mixes was assessed: one replacing steel fibres, and the others replacing aggregates and part of the cement. Furthermore, the two recycled UHPC mixes with recycled aggregates were evaluated using a multi-parameter approach. This approach emphasizes both mechanical and durability properties and examines their evolution under repeated damage and healing cycles. The details of the progressive mix design development are presented in Section §2, along with the microstructural characteristics of the recycled fine aggregates used in the mixes with cement replacement and the recycled fibres. Section §3 outlines the experimental programme, which includes preliminary characterization, initial and repeated induced damage, and a schematic overview of the curing periods. Section §4 provides an in-depth discussion of the main results and findings from the experimental campaign, emphasizing the significant potential of using parent UHPC to produce recycled UHPC. This claim is further discussed in Section §5, where a life cycle assessment (LCA) of the production and recycling process is conducted to explore the benefits and burdens of replacing virgin material with the one obtained from existing UHPC structures. Finally, the conclusions are summarized in Section §6.

2. Materials

The recycled Ultra-High Performance Concrete (R-UHPC) mixes used for the experiments reported in this paper were designed according to the formulation of the parent UHPC mix – indicated as REF – developed by Borg et al. [43] in the framework of the ReSHEALience project [44]. Borg et al. [43] first conceptualized the production of UHPC with aggregates recycled from the same mix. A tailored equipment was developed to adequately separate the steel fibres (L = 20 mm, Ø = 0.22 mm) from the cementitious matrix, and repeated crushing was needed to obtain particles with suitable fineness for UHPC production. The next step towards more sustainable UHPC production involved the partial replacement of either cement (30 %) or steel fibres (100 %). This approach leverages, on the one hand, the significant un-hydrated compounds present in the crushed parent UHPC [45]. On the other hand, the inherent durability and self-healing capacity of UHPC help protect the embedded steel fibres from corrosion. Consequently, an attempt was made to replace virgin steel fibres with recycled fibres extracted using a tailored recycling equipment featuring a magnetic separator. The mix containing recycled fibres (F100) was preliminarily assessed by Ferrara et al. [46], alongside two other mixes – both featuring 100 % recycled aggregates and a 30 % reduction in cement content: one using non-sieved recycled aggregates (C100C) and the other

Table 1
Mix design of the parent UHPC and different R-UHPC mixes; the mixes investigated in the present paper are underlined.

Constituent	REF	F100	C100C	C100F
	[kg/m^3]	[kg/m^3]	[kg/m^3]	[kg/m^3]
CEM I 52.5R	700	700	490	490
Silica fume	400	400	400	400
SP Glenium ACE 442	64	64	64	64
Water	231	231	231	231
Sand 117/F (Ø1.0–1.5 mm)	286	286	–	–
Sand 103 (Ø0.6–1.0 mm)	409	409	–	–
Sand 113 (Ø0.2–0.35 mm)	122	122	–	–
Steel fibres 20/0.22	160	–	160	160
Crystalline admixture	5.6	5.6	5.6	5.6
Recycled aggregates	–	–	1027	817
Recycled fines	–	–	–	210
Recycled fibres	–	160	–	–

incorporating sieved recycled aggregates and fines (C100F), preliminarily assessed by Davolio et al. [47]. Table 1 provides a summary of the different mixes described.

To prepare the R-UHPC mixes, the parent (REF) UHPC mix was cast at the University of Malta, and after 28 days of curing and three months of exposure in laboratory environment (20 °C, 50 % RH) it was crushed and separated through a multistage process. First, the parent UHPC mix was initially crushed using a jaw crusher. The resulting granules were then sieved with a 2.0 mm sieve to separate and remove any larger particles. The recycled fines are the residual fraction that passed through the finest sieve, with a 75 μm grid opening. The granulometric curve of the recycled material after the preliminary sorting is provided in Fig. 1 (dash-dot line). However, for the final mix the recycled aggregates were sorted to resemble the granulometric curve of the natural aggregates (Fig. 1, dashed line). Finally, the density of the recycled fines was determined according to the EN 196-6 [48], and it resulted equal to 2.482 g/cm^3. The fibres were extracted from the sieved material by using a magnetic separator.

Microstructural observations on the changes occurring in the UHPC mix when adding recycled particles or fibres were conducted after 28 days of standard curing to understand the microstructural differences occurring when using recycled materials. Scanning Electron Microscopy (SEM) pictures were taken at different magnification scales both on the reference UHPC mix and in the mix with recycled particles and additional fines content, as reported in Fig. 2. The SEM images highlight the effects of processing on the particles, particularly evident in Fig. 2d, where the rough surface of the mix with recycled fines indicates the presence of residual adhered mortar. The role of the mortar, particularly on capillary absorption, was extensively discussed in literature [49–51], and it will be further discussed in the present manuscript. However, the implications of potential latent hydration capacity provided by the inclusion of recycled UHPC are rather unexplored, and specifically the effectiveness of finer particles, and their contribution to self-healing of UHPC.

Additionally, the darker regions of the SEM pictures show the development of hydrates in both mixes. For the reference mix, Fig. 2b clearly shows the presence of needle-like phases, which are scarce in the mix with recycled fines. The latter (Fig. 2d) shows a more compact and homogeneous C-S-H formation, which correlates with better strength development.

Finally, the mix with recycled fibres was observed under SEM to evaluate the condition of the fibres after the crushing and sorting processes. The pictures obtained, reported in Fig. 3, show that, despite the multi-step separation process, the integrity of the fibres is preserved. Nonetheless, small scratches are visible on some of the fibres (Fig. 3b).

3. Experimental programme

The preliminary assessment on the mechanical performance of the three mixes with either cement and aggregates or fibres replacement is reported in Table 2. The latent hydraulic activity provided by the recycled particles in the mixes with recycled components enhanced compressive strength development, resulting in an increase of approximately +15 % after 120 days. This late stage strengthening aligns with SEM observations, which showed that the reference mix had reached maturity after 28 days, whereas the C100F mix still had potential for further microstructural buildup. Conversely, the flexural strength showed variability, largely due to the inherent randomness of fibre orientation within the small sections used for the three-point bending tests. However, the slight reduction in flexural strength observed in mixes with cement replacement should be considered when evaluating their feasibility for typical UHPC structures.

Beyond mechanical performance, the ability of these mixes to undergo autogenous healing is a key aspect to consider, as thoroughly discussed in the introduction. Given the crucial role of the cementitious phases in self-healing processes, the experimental program focused on assessing the healing capacity of C100C and C100F – the mixes with cement and aggregates replacement – in comparison to the reference mix (REF). Since F100 contained no cement replacement, its behaviour was expected to align with the reference and was therefore not investigated separately. Therefore, the experimental program was designed to assess the self-healing capacity of the mixes, considering both mechanical and durability performance, with a specific focus on damage recovery. A total of

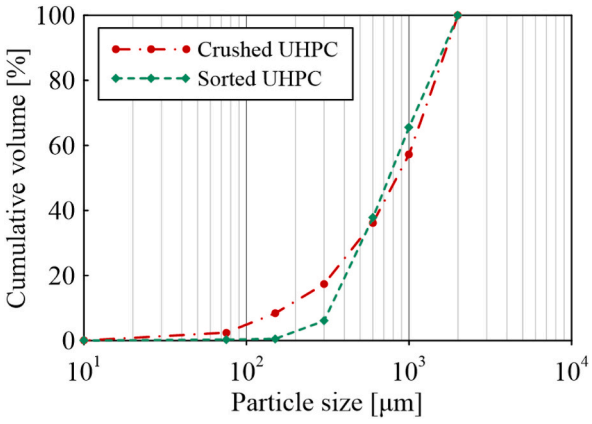

Fig. 1. Granulometric distribution of the crushed UHPC and granulometric curve adopted for the mixes, equal to the granulometry of the natural aggregates of the original (parent) mix.

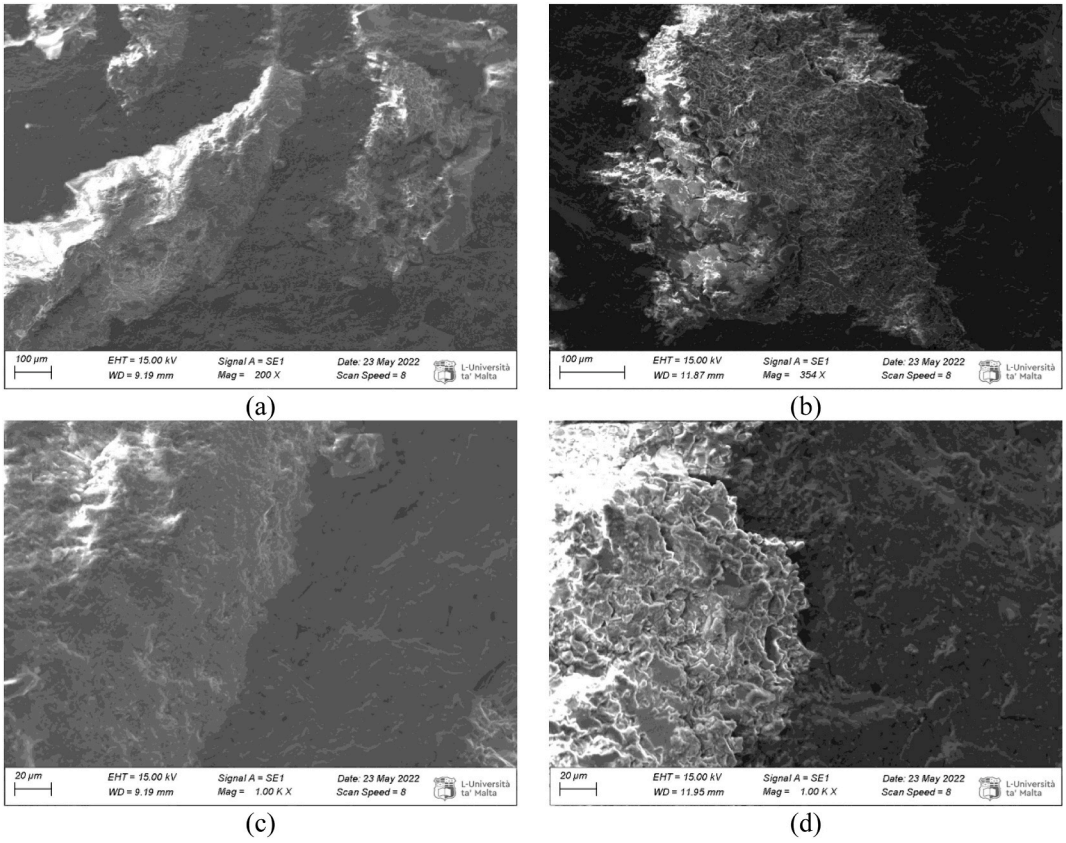

Fig. 2. Comparison between the microstructure of (a, c) the reference mix, and (b, d) the mix C100F with recycled aggregates and fines; the SEM pictures highlight the rough superficial structure of the R-UHPC mix.

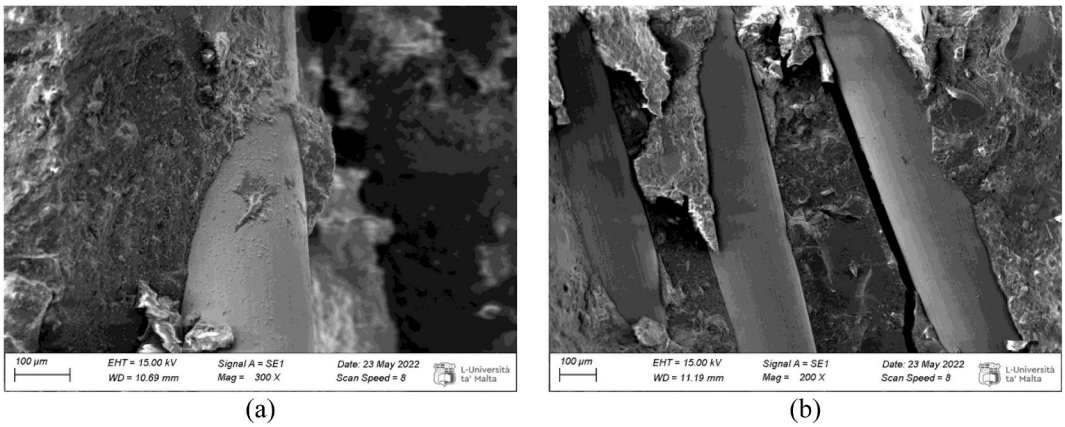

Fig. 3. Scanning Electron Microscopy of the mix F100 with recycled fibres; the integrity of the steel fibres is preserved, despite minor scratches on the surface.

twelve (12) prismatic specimens, each measuring 40 × 40 × 160 mm, were cast for each mix. The summary of the experimental campaign is represented in Fig. 4. To start with, the mechanical performance of the mixes was assessed both in compression and bending (Group 1). Then, an initial damage was induced on the samples, which were subsequently exposed to a chloride solution (3.3 % NaCl) that represents the marine environment. At fixed times, mechanical and durability tests were repeated on the samples to assess the variation of the performance due to the self-healing process. For some specimens (Group 2), the healing process inside the exposure tank was carried out continuously. Conversely, the remaining specimens (Group 3) were repeatedly damaged after each exposure time. Half of the specimens from Group 3 was tested to failure after the third month, while the other half prolonged the exposure time until

Table 2
Mechanical performance of the mixes at 28 days and 120 days of ageing.

Mix	Compressive strength f_c [N/mm^2]		Flexural strength f_{fl} [N/mm^2]	
	28 days	120 days	28 days	120 days
REF	135.47 (±5 %)	155.69 (±27 %)	34.43 (±25 %)	31.88 (±13 %)
F100	124.25 (±5 %)	177.51 (±5 %)	23.62 (±4 %)	29.09 (±16 %)
C100C	149.78 (±3 %)	184.72 (±10 %)	27.38 (±4 %)	26.52 (±11 %)
C100F	136.75 (±5 %)	180.37 (±5 %)	26.75 (±6 %)	22.40 (±21 %)

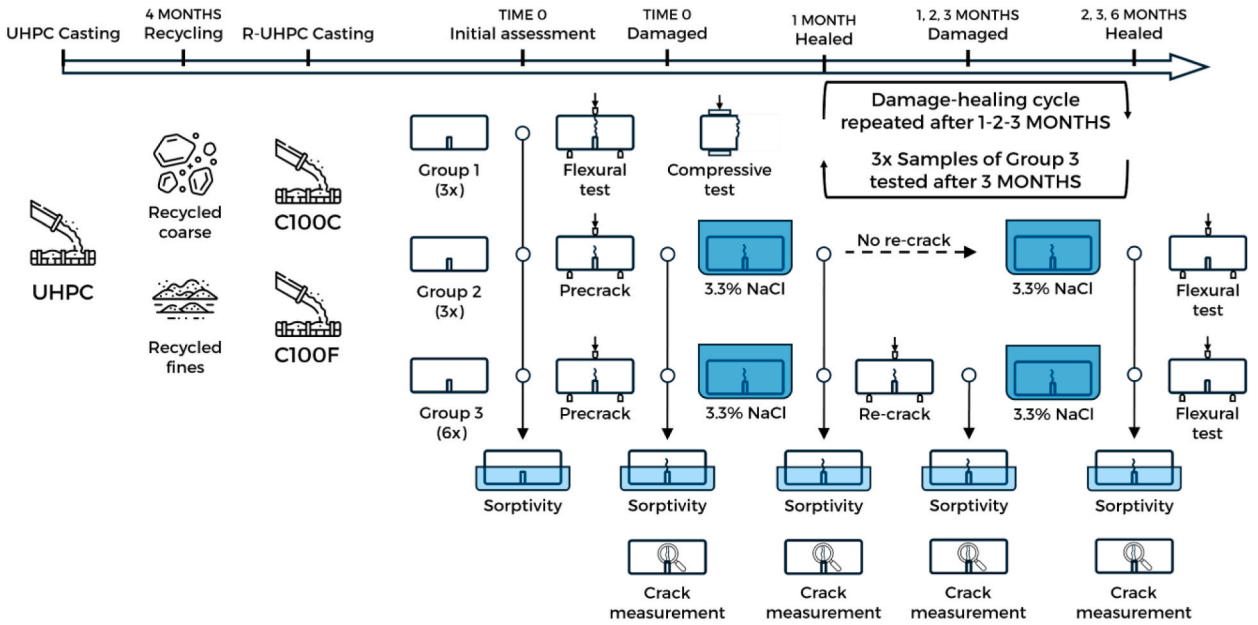

Fig. 4. Schematic representation of the experimental campaign; Group 1 served as preliminary assessment, Group 2 was continuously healed after the initial damage, and Group 3 was repeatedly damaged over time.

the sixth month, when they were tested together with Group 2. In addition to the two mixes with recycled components, the self-healing capacity of the reference mix was assessed, focusing solely on initial damage and progressive recovery.

3.1. Three-point bending tests

The 40 × 40 × 160 mm R-UHPC prisms were subjected to three-point bending (3PB) tests to characterize the flexural response. To localize cracking during bending tests, a notch was cut across the bottom surface of each prism. The notch was centrally positioned, with a length of 8 mm and an approximate width of 2 mm. The tests were conducted in actuator vertical displacement control at 0.5 μm/s speed. During the tests, Crack Mouth Opening Displacement (CMOD) measurements were recorded through a clip-on gauge positioned on the bottom surface of the sample, across the notch. The nominal flexural stress (σ_{fl}) is determined according to Eq. (1).

$$\sigma_{fl} = \frac{3 \times P \times L}{2 \times b \times d^2} \tag{1}$$

where P is the applied load [N], L is the distance between the supports [mm], b is the notched section depth [mm], and d is the notched section height [mm]. Compressive strength tests were then performed on the resulting halves obtained from the flexural tests, according to EN 1015–11:2019 [52].

For the specimens used to assess the self-healing capacity, the initial damage was induced on the prismatic samples by means of the same three-point bending tests, and a target crack mouth opening displacement (CMOD) of 150 μm was reached. The target CMOD value is measured when the load is applied on the small beam, and, thus, the actual crack width differs from the target due to the elastic recovery after unloading.

The stress-CMOD curves from both pre-cracking and re-cracking phases were analysed to evaluate changes in stiffness due to damage-healing cycles. To quantify these changes, two Indices of Stiffness Recovery (ISR) were introduced, following the approach outlined by Lo Monte et al. [20]. Loading stiffness ($K_{loading}$) was determined as the slope of the initial segment of the curve, specifically identified as the portion between 5 % and 20 % of the maximum flexural stress observed during the cracking process. In contrast,

unloading stiffness ($K_{unloading}$) was calculated as the secant slope of the unloading curve, spanning from the point of maximum CMOD to the point where the residual stress reaches zero. An example on the calculation of the two stiffness values is provided in Fig. 5. One index (ISR_0, Eq. (2a)) quantifies the change in stiffness relative to the pre-cracking phase, when damage is initially applied to the intact material. The second index (ISR_Δ, Eq. (2b)) measures variations with respect to the previous cracking phase, specifically each re-cracking cycle. This second index was applicable only to samples that underwent repeated damage (i.e., Group 3).

$$ISR_0 = \frac{K_{loading}^{j-month} - K_{unloading}^{precracking}}{K_{loading}^{precracking} - K_{unloading}^{precracking}} \tag{2a}$$

$$ISR_\Delta = \frac{K_{loading}^{j-month} - K_{unloading}^{(j-1)-month}}{K_{loading}^{(j-1)-month} - K_{unloading}^{(j-1)-month}} \tag{2b}$$

Finally, the fracture response of the mixes was considered. The work of fracture (WoF) was calculated as the integral of the stress-CMOD curve up to the fixed value of 1.5 mm CMOD on the failure curve of each specimen (Eq. (3)). This value corresponds to a nominal strain at the bottom fibre of approximately 5 %, indicating full yielding of the steel reinforcement in a conventional reinforced concrete beam, nearing the ultimate limit state (ULS).

$$WoF = \int_0^{1.5\ mm} \sigma(CMOD)dCMOD \tag{3}$$

3.2. Crack measurements

After inducing initial damage through a three-point bending flexural load, the cracks on the two lateral surfaces of the prisms were examined using a digital microscope. For Group 2 samples, observations were repeated after each exposure period, while for Group 3 samples, an additional observation was conducted following each re-cracking process. It is important to note that when the specimen is unloaded, elastic recovery causes partial closure of the formed crack. Consequently, the measured crack width under unloaded conditions differs from the target crack opening, which corresponds to the width measured under the applied load. Additionally, the crack width is calculated as the average width along the crack profile, determined by the ratio of the crack area to its longitudinal development. This approach further distinguishes the measured width from the target width, which is taken specifically at the bottom of the sample. The crack profile was acquired as a sequence of pictures taken with the digital microscope (Dino-Lite Model AM4113T). Then, the microscope images were merged using the commercial software Adobe Photoshop to reconstruct the full profile of the crack (Fig. 6a). Finally, the image was binarized, converting it from full colour to a grayscale representation where the crack profile appears as white against a grey background (Fig. 6b). Then, the crack area on the two sides of the samples was measured.

The variations in crack size over time reflect the impact of the crack self-sealing process, making the crack area a key benchmark for quantifying self-sealing and self-healing efficiency. To measure this, the Index of Crack Sealing (ICS) was introduced, which quantifies the proportion of the initial crack that has been successfully sealed. For each sample, the ICS was calculated separately for both sides of the crack, and the average of these values was used. For samples that were only pre-cracked and underwent continuous undisturbed healing, the index is calculated based on the ratio between the crack area at a given month and the area of the same crack measured immediately after pre-cracking (ICS_0, Eq. (4a)). In contrast, for samples subjected to repeated cracking over different time periods, the index is defined relative to the previous month's crack area (ICS_Δ, Eq. (4b)). This approach allows for an assessment of the repeatability of the healing processes when the material undergoes multiple loading-unloading cycles. The index is equal to 0 when the area of the crack after curing is the same as the reference value (i.e., no healing occurred), while it is equal to 1 when the crack is completely sealed and, therefore, the final area of the crack is 0 mm^2.

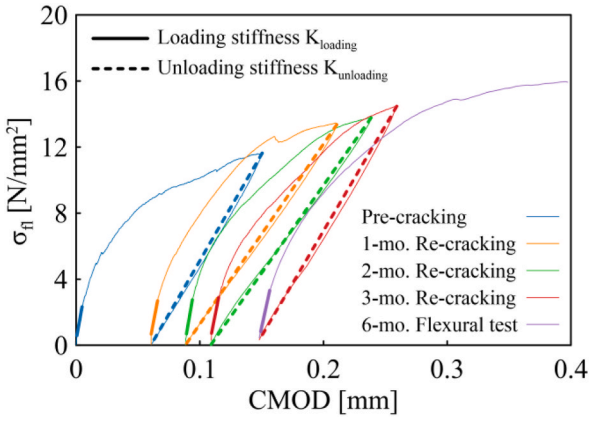

Fig. 5. Methodology adopted to calculate the loading and unloading stiffness at each time step for the Index of Stiffness Recovery.

Fig. 6. Crack along the sample's side (a) as taken with the microscope and merged, and (b) after binarization.

$$ICS_0 = 1 - \frac{A_{cured}^{j-month}}{A_{precracking}} \tag{4a}$$

$$ICS_\Delta = 1 - \frac{A_{cured}^{j-month}}{A_{recracked}^{(j-1)-month}} \tag{4b}$$

3.3. Sorptivity tests

The durability assessment consisted of sorptivity measurements on the notched prismatic samples, conducted according to ASTM C1585-20 [53]. The procedure was adjusted to account for the different geometry of the specimen, as proposed by Cuenca et al. [54]. A silicon layer was applied to the sides and bottom of the samples, restricting water absorption to the central portion of the prism. Specifically, a 20 mm wide section was left unsealed to focus absorption around and across the notch. The water level was maintained at approximately 10 mm above the specimen's base, fully submerging the notch and extending 2–3 mm beyond it (Fig. 7).

The absorption was calculated as the ratio between the change in mass (m_t) at the time t and the exposed area of the specimen (a) multiplied by the water density (d), assumed equal to 0.001 g/mm^3 (Eq. (5)). The absorption is thus expressed in [mm].

$$\text{Absorption} = \frac{m_t}{a \times d} \tag{5}$$

The rate of water absorption, also called sorptivity (S), was then determined as the slope of the curve that correlates the absorption with the square root of time up to 6h, and it is expressed in [mm/s$^{0.5}$]. The obtained sorptivity rate depends on the crack opening at the tip of the notch, which is affected by the induced damage and subsequent healing periods. Therefore, the index of sorptivity healing

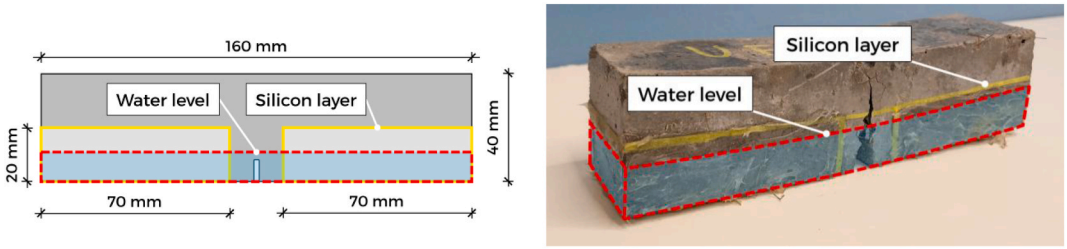

(a) (b)

Fig. 7. Layout of the sorptivity test (a) schematically represented, and (b) on a sample.

(ISH) was introduced to quantify the impact of the healing process on the capillary absorption of the samples. Similarly to the ICS, sorptivity healing is calculated separately for pre-cracked samples – based on the ratio of sorptivity at a given month to the sorptivity measured immediately after pre-cracking (ISH_0, Eq. (6a)) – and for samples subjected to repeated cracking over time, defined relative to the sorptivity of the previous month (ISH_Δ, Eq. (6b)).

$$ISH_0 = 1 - \frac{S_{cured}^{j-month}}{S_{precracking}} \tag{6a}$$

$$ISH_\Delta = 1 - \frac{S_{cured}^{j-month}}{S_{recracked}^{(j-1)-month}} \tag{6b}$$

4. Results and discussion

This section presents the results obtained from the experimental campaign conducted on the C100C and C100F mixes, both featuring a partial reduction of cement content replaced by recycled UHPC unsorted or sorted fines. The outcomes are discussed in terms of self-healing performance, with a direct comparison to the reference mix (REF), including observations on healing performance under repeated damage and healing cycles.

4.1. Crack sealing

The filling of the cracks due to the formation of healing products is the basic indication of the self-healing efficiency of the material, and it can be directly observed on the specimens. Fig. 8 shows the progressive closure of the crack on a sample made with recycled coarse aggregates (C100C) that was initially pre-cracked and then exposed to the chloride solution for six months. Specifically, the three figures represent the crack in its initial state (Fig. 8a), after one month of exposure (Fig. 8b), and after three months of exposure (Fig. 8c). The binary processing clearly shows that the crack profile is significantly reduced after just one month of exposure, with the material being able to seal the thinner parts of the crack in a short period of time. As the healing process advanced, the crack area was further diminished, and after three months the crack was completely sealed.

The self-sealing capacity of the two mixes is highlighted in Fig. 9 and compared to the reference. As it can be observed in Fig. 9a, the residual crack area was halved in the first month of exposure. This is consistent with the results described by Xi and Ferrara [55], since most of the self-healing for UHPC takes place in a short time span due to the higher availability of unhydrated cement particles exposed to water upon the cracking process. The crack closure proceeded undisturbed for the subsequent periods following an almost constant rate. However, since the mix with recycled coarse aggregates achieved almost 90 % of closure in two months, the healing slowed down, likely because of the same closure of the cracks which hindered further penetration of water inside the cracks and the consequent hydration of unhydrated binder; as a result, complete crack closure could be achieved only after six months. Conversely, the other mix always featured lower healing rates, and the cracks were not completely sealed within the investigated time span. As observed by Duan et al. [56], recycled fines have limited $CaCO_3$ precipitation due to the size and interface of the grains with respect to coarser recycled aggregates. Not only did coarser aggregates foster the production of precipitates, but the single-grain repair products exhibited better

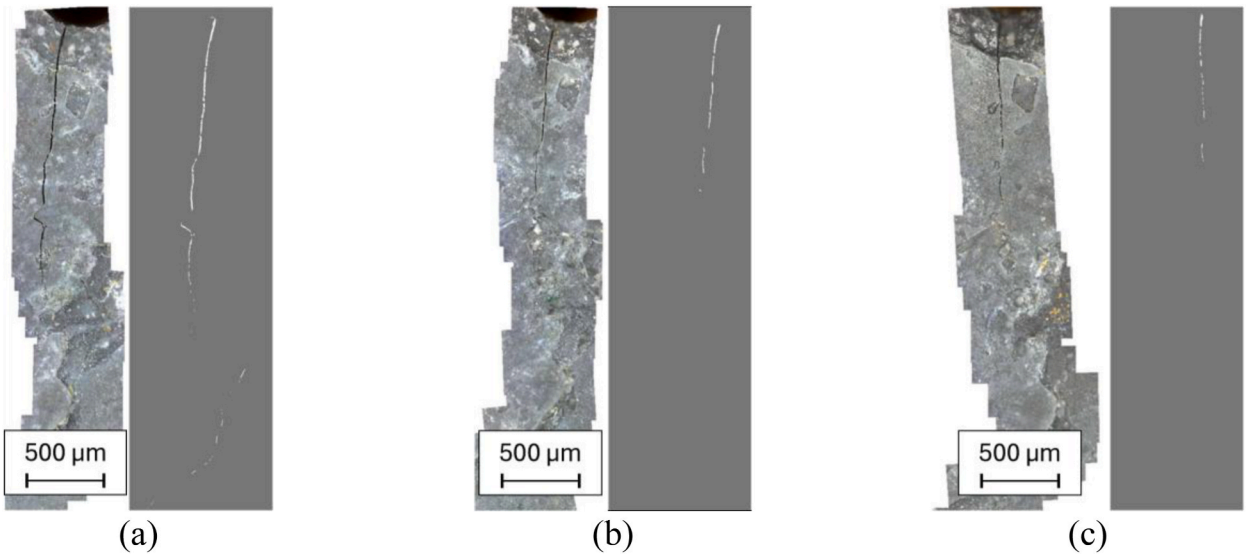

Fig. 8. Crack opening profile on a pre-cracked sample with recycled coarse aggregates (C100C); (a) after pre-cracking, (b) after one month, and (c) after two months.

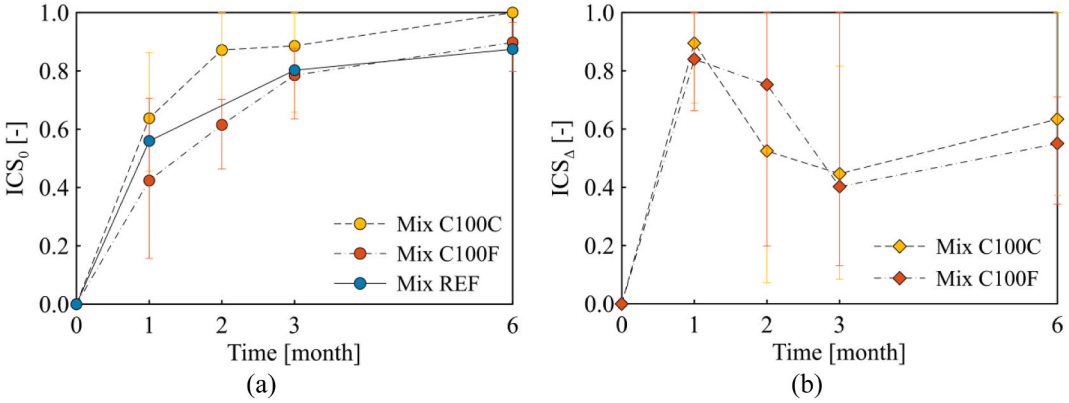

Fig. 9. Index of crack sealing (ICS) over time for the mixes; (a) pre-cracked samples, and (b) samples re-cracked at each time step.

filling, which explains the improved crack closure observed in Fig. 9.

The observed crack sealing behaviour in R-UHPC mixes, surpassing that of the reference mix by the end of the exposure period, can be attributed to the additional unhydrated mortar introduced by recycled UHPC. This residual mortar enhances the precipitation of calcium carbonate, particularly in cracks with smaller initial widths [36]. However, as cracks narrow over time – especially after approximately three months – precipitation kinetics slow down, as previously discussed by Medjigbodo et al. [42]. This reduction in reaction rate can, in some cases, prevent complete crack closure. Additionally, the self-healing efficiency diminishes under repeated damage cycles, as evident in both C100C and C100F mixes (Fig. 9b). While the extended final exposure period partially mitigates this decline by allowing more time for precipitation, the progressive reduction in healing potential suggests a fundamental limitation: although the old adhered mortar contributes to crack repair in early cycles, sustained self-healing requires a continuous source of unhydrated cement. Furthermore, the slightly higher sealing efficiency observed in the R-UHPC mixes compared to the reference mix confirms that the less dense microstructure resulting from the presence of recycled aggregates may facilitate the diffusion-precipitation process [57]. These findings highlight the need to optimize mix design strategies to balance initial self-healing efficiency with long-term durability under cyclic loading.

In addition to examining crack sealing over time, the graph in Fig. 10 correlates the observed closure with the initial crack width measured using the digital microscope. Despite significant data scatter, a clear decreasing trend is evident across all cases, indicating the increasing difficulty of autogenous healing in sealing wider cracks. This limitation can be attributed to the lower availability of calcium ions and hydration products for crack bridging, as well as the reduced capillary forces driving precipitation in larger voids [58]. Furthermore, the trend lines associated with repeated cracking exhibit a slightly steeper slope (-3.95×10^{-2} vs. -2.98×10^{-2}) compared to specimens that were only pre-cracked, suggesting that the healing efficiency declines with successive damage cycles. This reduction is likely due to the depletion of unhydrated cementitious phases and the reduced reactivity of recycled material, which may hinder the formation of new hydration products necessary for sealing. These findings reinforce the idea that while self-healing is a promising mechanism for enhancing durability, its effectiveness is inherently constrained by material composition and damage history.

4.2. Sorptivity healing

The direct observation on the lateral cracks provides only a superficial understanding of the healing phenomenon, which must

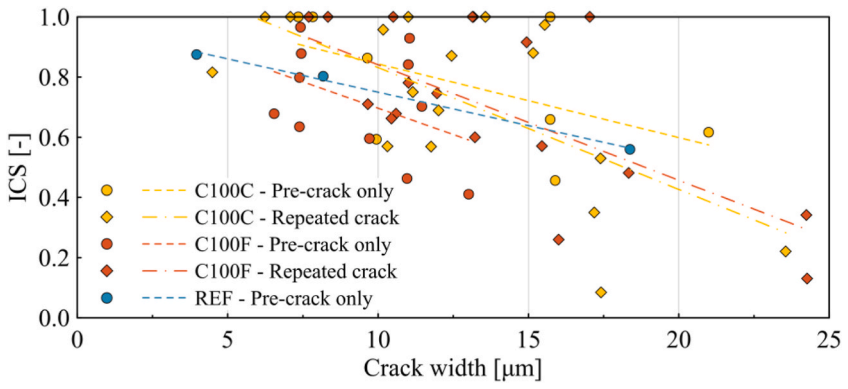

Fig. 10. Index of crack sealing (either ICS$_0$ or ICS$_\Delta$) as a function of the initial crack width for the mixes.

henceforth be assessed through multiple parameters, as suggested, for instance, by Lo Monte et al. [20]. The most used non-destructive method to evaluate the closure of the cracks formed on the bottom surface of a sample is the water absorption test [54,59]. The sorptivity rate is governed by capillary absorption, which, in turn, directly depends on the surface area in contact with water. The reduction in sorptivity due to self-healing can thus be associated with the precipitation of particles that, on the one hand, limit the surface availability for capillary rise and, on the other hand, increase the tortuosity of the crack [60,61].

The recovery observed in terms of reduced sorptivity for the mix with recycled unsorted aggregates (C100C) confirms its remarkable capacity to fill the crack volume within a short period (Fig. 11a). This rapid healing can be attributed to the presence of unhydrated cementitious phases within the recycled UHPC, which promote precipitation and densification of the damaged regions. Although complete healing is not achieved due to the definition of the index (see §3.3), the final sorptivity rate after six months of exposure is reduced to one-fifth of its initial value after pre-cracking, demonstrating the efficiency of the healing mechanism in reducing permeability.

Conversely, when recycled fines are incorporated into the mix (C100F), a higher inherent water absorption is observed, leading to limited sorptivity recovery [62]. This behaviour can be linked to the increased porosity and capillary rise associated with the finer recycled particles, which hinder the precipitation-driven healing process. The reference mix, on the other hand, exhibited an intermediate performance, reinforcing the idea that replacing cement with recycled aggregates from a parent UHPC mix can be an effective method for enhancing crack closure. However, the presence of additional fine fractions appears to counteract this benefit by introducing a more porous microstructure and increasing transport properties [63].

Repeated damage-healing cycles resulted in a sorptivity recovery trend that closely aligns with the crack sealing observations for both the C100C and C100F mixes, confirming the limitations of these mixes in successive recovery cycles. This limitation suggests that while self-healing mechanisms are effective in the early stages of exposure, their potential is constrained by the availability of reactive phases. The performance observed for all mixes, as shown in Fig. 11b, highlights the role of recycled aggregates in contributing to higher water absorption [64] According to the study by Qian et al. [41], an excess of fine recycled particles may lead to increased defect formation in the matrix, negatively impacting the overall durability of the mix. In the case of C100F, this observation suggests that the amount of cement replacement might exceed the optimal threshold for maintaining durability integrity. While Qian et al. [41] identified an optimal replacement level at 25 %, the 30 % replacement used in the present study may have led to a suboptimal balance between sustainability and performance, ultimately limiting the efficiency of the self-healing process.

Although sorptivity recovery is observed, it should be substantiated by the absolute sorptivity values, as they provide a clearer indication of actual durability performance. The sorptivity of the mixes incorporating recycled UHPC was higher than that of the reference mix, regardless of exposure time or conditions (Fig. 12a). These findings underscore the challenges associated with adopting high replacement rates. Nevertheless, even after six months of exposure to the chloride solution, the steel fibres in the cross-section of the small beams showed no visible rust on their surface (Fig. 12b). This suggests that, despite the high water absorption rates observed in the sorptivity test, the density of the UHPC matrix, combined with the precipitation of healing particles during cracking, effectively protects the fibres from chemical attack.

4.3. Stiffness recovery

The stiffness recovery provides insight into the healing efficiency with respect to the mechanical response of the material, specifically in the elastic range, as the stiffness is calculated between 5 % and 20 % of the maximum load reached during the cracking process. Although the flexural response of the material is non-linear, it can reasonably be approximated by a linear pattern along the first branch of the curve, which is then compared to the initial elastic stiffness.

When the stiffness recovery index approaches 100 %, it suggests that the precipitates formed during the autogenous healing process are effectively bridging the two halves of the original crack restoring the structural continuity of the material through the crack, allowing the same material to recover its pristine mechanical integrity. Furthermore, in some cases, the precipitates provide additional

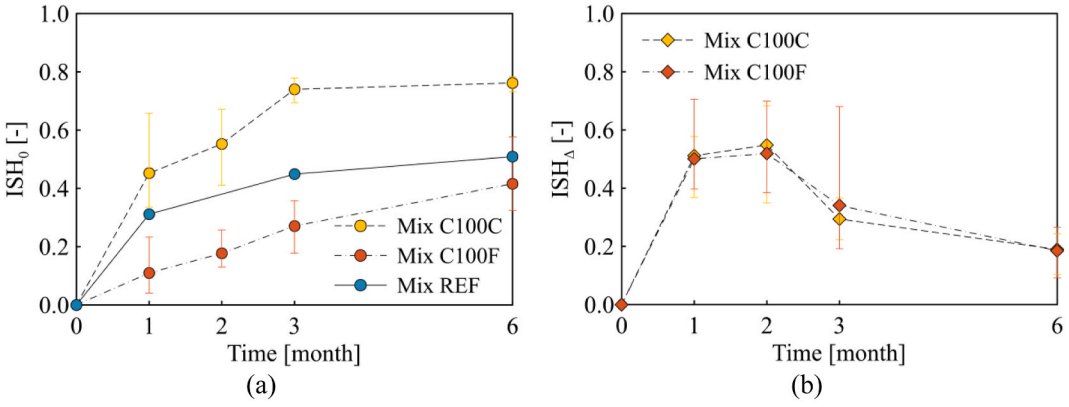

Fig. 11. Index of sorptivity healing (ISH) over time for the mixes; (a) pre-cracked samples, and (b) samples re-cracked at each time step.

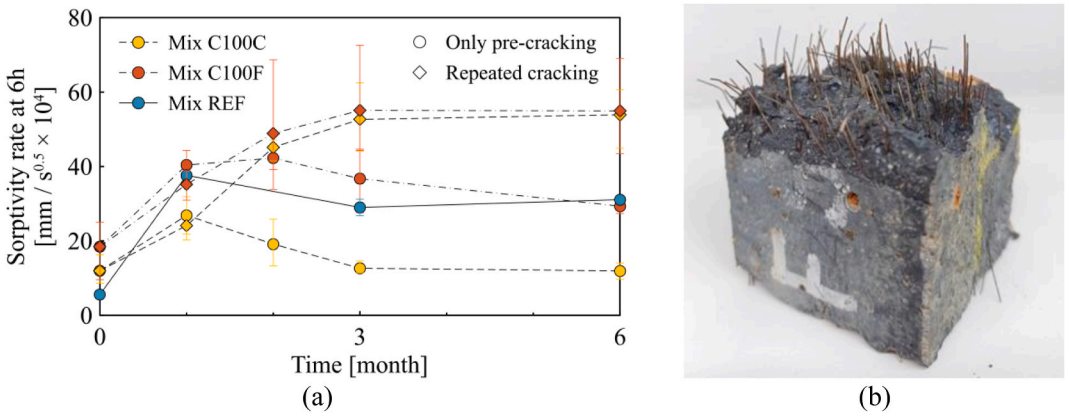

Fig. 12. (a) Sorptivity rate of the mixes over time, either for pre-cracked or repeatedly cracked samples, and (b) detail of the fibres in the cross-section of a pre-cracked C100C sample after six months of exposure to a 3.3 % NaCl solution; visible rust is observed on the surface, where the steel sections of the fibres were directly exposed to the environment, while the embedded fibres remain free of rust.

stiffness relative to the material's undamaged state. Such behaviour, already observed in similar experimental investigations [65], underscores the potential of autogenous healing to enhance the mechanical performance of the material beyond its original state.

The graph in Fig. 13a illustrates the stiffness recovery observed after six months of exposure in pre-cracked specimens. Despite variations in crack closure efficiency, the effectiveness of the precipitates in preserving the material elastic response appears comparable across the investigated R-UHPC mixes. Notably, both recycled mixes achieved full stiffness recovery within the exposure period and even exhibited, on average, an increase in stiffness, a phenomenon previously observed by Alameri et al. [66]. This increase could be attributed to the densification of the crack interface through continued hydration of unreacted cementitious phases and the precipitation of calcium carbonate, which contribute to enhanced load transfer. Particularly, the increased contact area provided by the recycled aggregates improved the interface bonding, as discussed by Liu et al. [67]. In contrast, the reference mix exhibited significantly lower stiffness recovery, suggesting that the bonds formed by healing precipitates were not sufficiently robust to restore stiffness in the elastic range. The superior performance of the R-UHPC mixes highlights the role of adhered mortar from recycled UHPC in promoting a more effective healing process.

When repeatedly cracked, the samples demonstrated the ability to compensate for the damage in all instances, achieving at least 70 % recovery (Fig. 13b). Notably, the damage-healing cycles produced stiffness recovery index values exceeding 100 % after one month for the C100F mix (with additional fines) and after both one and two months for the C100C mix (with unsorted aggregates). During the third exposure period, the healing process resulted in only partial recovery – approximately 80 % for both mixes –, reflecting the limited repeated healing capability of the investigated mixes. The combined effect of additional induced damage and longer exposure period (three months) yielded, after six months, a performance comparable to that of the previous step, possibly driven by the enhanced fibre-matrix bond associated with the healing process [68]. Nonetheless, repeated cracking cycles might impair the recovery capacity at the fibre-matrix interface.

4.4. Flexural performance and fracture properties

The healing process described and quantified in the previous sections is directly reflected in the results of the flexural tests, which

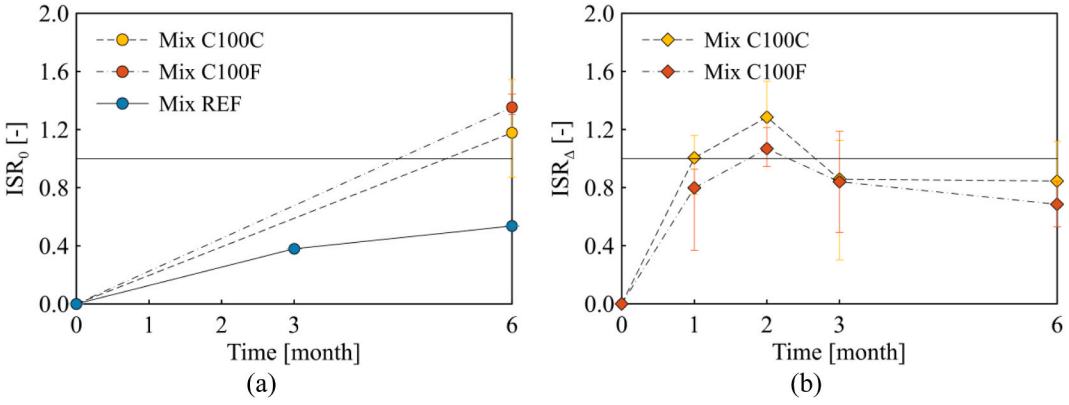

Fig. 13. Index of stiffness recovery (ISR) over time for the mixes; (a) pre-cracked samples, and (b) samples re-cracked at each time step.

assess the macroscopic response of the material. By evaluating flexural behaviour under various conditions, these tests reveal how the healing mechanisms influence the material's structural performance. As shown in Fig. 14a, the initial flexural response of the mix containing unsorted aggregates constitutes, on average, the lower boundary of the envelope of the curves. This indicates that, after damaging the specimens and exposing them to the chloride solution, the process of crack sealing could restore the continuity of the material and effectively provide a bridging effect across the damaged surfaces. An additional contribution to the flexural strength after damage and healing is provided by the steel fibres. Specifically, the fibre-matrix interface can benefit from self-healing due to the densification in the damaged zone and the deposition of particles within the cracked area [69]. Furthermore, immersion in a chloride solution appears to enhance the fibre-matrix interface. This phenomenon, already observed by Al-Obaidi et al. [68], is likely due to increased surface roughness from corrosion and the formation of rust crystals [70].

Similarly, the mix with additional fines exhibited consistent performance across all scenarios (Fig. 14b). The incomplete healing is evident in the slightly lower strength enhancements observed in the damaged and cured specimens compared to the preliminary characterization, which serves as the reference. Nonetheless, most curves, particularly those for the pre-cracked specimens, outperformed the undamaged samples. An outlier was observed in the flexural tests after three months. This deviation was attributed to variability of fibre content and orientation, a factor that is particularly critical for small-sized beams.

The evolution of peak flexural strength reported in Fig. 15a highlights the superior initial performance of the reference mix, which, on average, matched the best results obtained for the R-UHPC mixes. However, after six months of exposure, all mixes exhibited comparable performance, reinforcing the long-term benefits of incorporating recycled aggregates from a parent UHPC, as previously discussed. This convergence suggests that while the reference mix initially benefits from a denser microstructure and higher early-age strength, the sustained self-healing and hydration mechanisms in R-UHPC allow it to reach similar performance levels over time.

Among the R-UHPC mixes, the one with unsorted aggregates (C100C) demonstrated the highest peak flexural strength, with a slight increase observed in repeatedly cracked specimens, likely due to further densification at the crack interface. Similarly, the mix incorporating additional fines (C100F) showed a moderate performance enhancement after six months, despite highly scattered results at the intermediate (i.e., three-month) assessment. This variability may be attributed to the increased heterogeneity introduced by the finer recycled particles, which can influence both the crack healing dynamics and load redistribution within the material.

Overall flexural behaviour is more effectively characterized by the Work of Fracture (WoF), shown in Fig. 15b. This parameter is particularly relevant for UHPC structures, as they may experience significant deformations [23] and must maintain flexural strength even at large crack openings.

Although the long-term results exhibited a similar slight reduction in peak stress, the two mixes with cement replacement (C100C, C100F) demonstrated notable benefits from the damage-healing cycles. These cycles enhanced the flexural response due to the self-healing process discussed in previous sections. Notably, the mix with unsorted aggregates (C100C) consistently achieved a WoF comparable to the reference mix, even under repeated damage. Since this phenomenon is closely tied to the fibre-matrix interface [71,72], particularly at high deformation values considered in the WoF calculation (up to 1.5 mm), these results suggest that self-healing significantly improved the bridging effect provided by the steel fibres.

Conversely, the mix with additional fines (C100F) only partially compensated for its initial difference from the reference mix. It performed better in specimens subjected to pre-cracking alone, highlighting its reduced capacity to resist repeated damage cycles.

4.5. Healing indices cross-comparison

This section examines the cross-comparison of two indices reflecting macroscopic healing performance – namely, the index of sorptivity healing (ISH) and the index of stiffness recovery (ISR) – with crack closure observations captured via microscopy and expressed through the index of crack sealing (ICS). Fig. 16 illustrates comparisons for specimens that were only pre-cracked (Fig. 16a–c) and for those subjected to repeated damage (Fig. 16b–d).

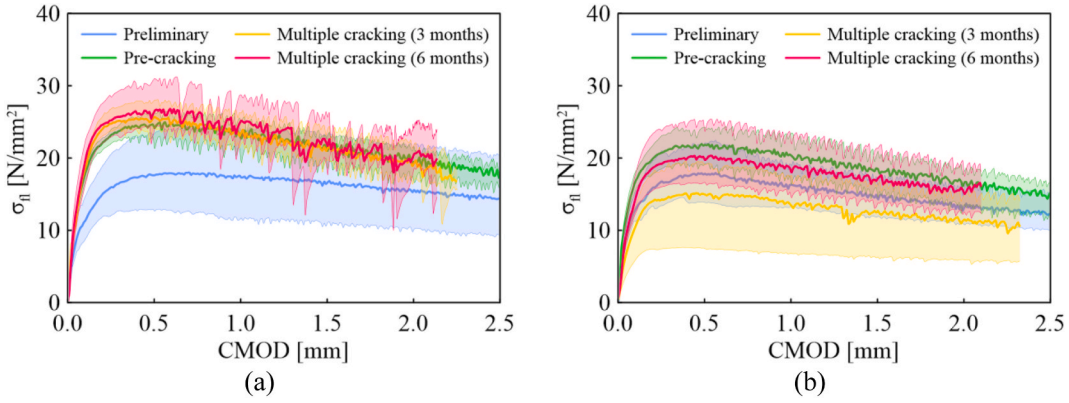

Fig. 14. Three-point bending experimental curves of all the specimens; (a) Mix C100C with recycled unsorted aggregates, and (b) Mix C100F with recycled fines.

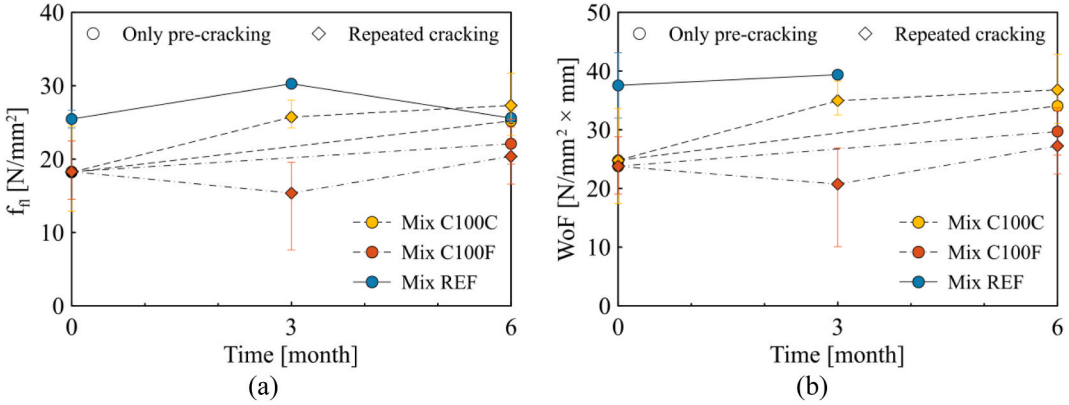

Fig. 15. Flexural response obtained with the three-point bending tests for the mixes, either pre-cracked or repeatedly cracked, where (a) represents the flexural peak stress and (b) the work of fracture; time 0 is referred to the preliminary characterization.

It is important to note that the definitions of these indices significantly influence their comparisons. For instance, a 100 % value in the sorptivity healing index would require the post-healing sorptivity rate to be zero, a condition that is hardly physically attainable. Consequently, the ISH values are slightly lower than the ICS values, as evident in Fig. 16a. Despite achieving comparable crack sealing values, mix C100F exhibited inherently higher sorptivity due to the presence of additional fines, as extensively discussed in Section §4.2. Nevertheless, the stiffness recovery provided by the healing products indicates effective mechanical recovery in all R-UHPC cases

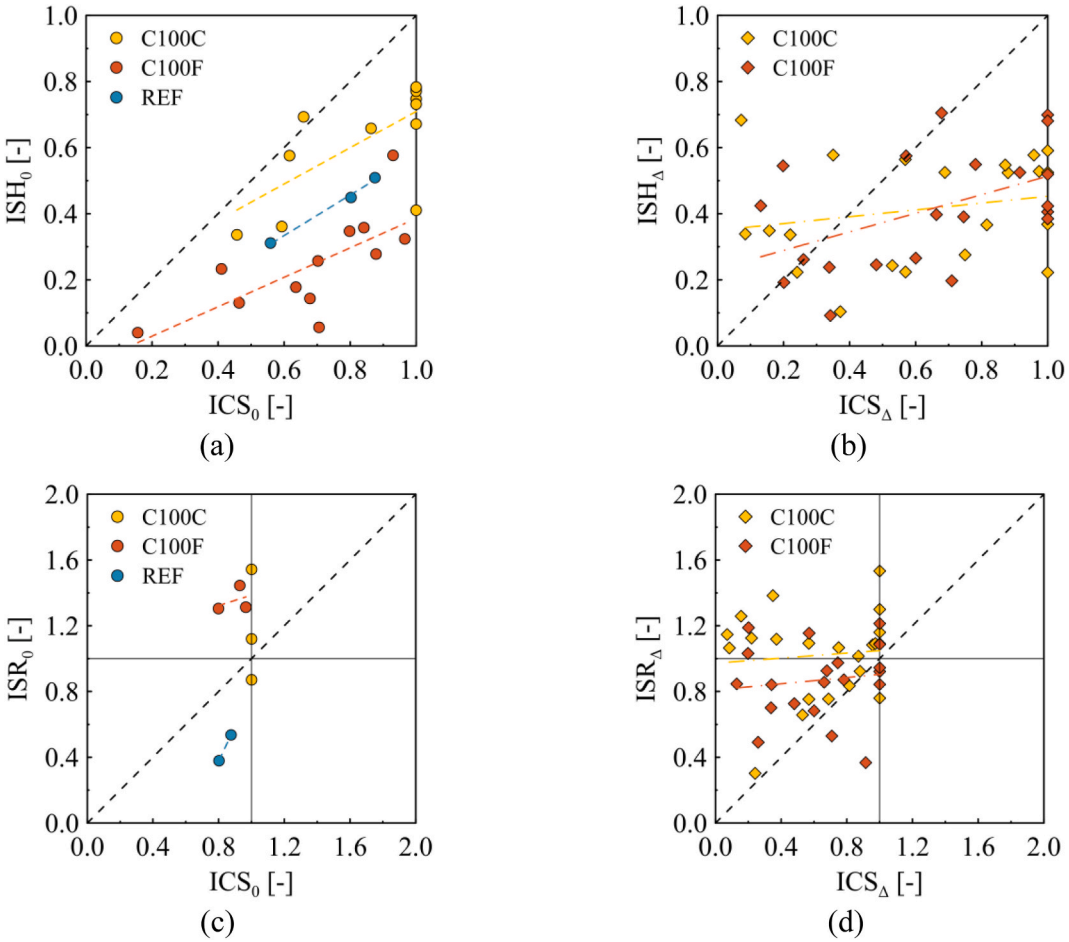

Fig. 16. Correlation between the index of crack sealing (ICS) and the indices of sorptivity healing (ISH) and stiffness recovery (ISR), respectively for (a,c) pre-cracked specimens, and (b,d) repeatedly cracked specimens.

(Fig. 16c). In contrast, the reference mix exhibited poor stiffness recovery, likely due to incomplete healing and, more importantly, the lower bond strength of the healing products compared to those formed in the R-UHPC mixes. This distinction highlights a key difference in the correlation between crack closure and stiffness recovery: while R-UHPC mixes not only achieved significant crack sealing but also translated it into a high level of stiffness restoration, the reference mix demonstrated a weaker correlation, with stiffness recovery lagging behind crack closure. This suggests that, in the reference mix, the precipitated healing products, although sufficient to fill cracks, were not mechanically robust enough to restore the elastic response. Conversely, in the R-UHPC mixes, the presence of weaker interfaces initially results in a less dense structure. This very characteristic promotes the formation of a more interconnected network during the healing process, as the precipitates progressively bridge cracks and reinforce the matrix [73].

For specimens subjected to repeated cracking, the indices confirmed the limited ability of both mixes to withstand multiple healing cycles. While crack sealing values ranged from 10 % to 100 %, sorptivity healing remained bound in most cases to the value achieved in the first healing period, as demonstrated by the lower slope of trend lines in Fig. 16b compared to Fig. 16a. Conversely, stiffness recovery displayed significant scatter (Fig. 16d), with values often lying above the diagonal. This is primarily attributable to the definition of the ISR, which emphasizes the re-loading stiffness – a parameter reflecting the steeper initial segment of the flexural response curve, rather than its subsequent, more gradual sections.

These findings anyway suggest that even under repeated damage, both R-UHPC mixes can maintain a robust structural response, despite incomplete crack sealing. This behaviour may be linked to the enhancement of the fibre-matrix interface, which, though not directly visible, plays a critical role in the flexural performance of the small beams.

4.6. Thermogravimetric analysis

A thermogravimetric analysis (TGA) was conducted on the reference mix (REF) and the mix with recycled components (C100F) to complement the mesoscale observations on mechanical and durability performance and to provide insight into the hydration and carbonation processes associated with the recycled constituents. The tests were performed using a Mettler Toledo TGA/DSC 1 machine in the range 20–1200 °C, with a heating rate of 10 °C/min and nitrogen as purge gas.

The results, reported in Fig. 17 as both weight loss and differential thermal analysis, show that the C100C specimen exhibited more pronounced mass losses across all the main transformation ranges, namely C-S-H dehydration (100–150 °C), portlandite dihydroxylation (450 °C), and calcium carbonate decomposition (600–800 °C). These results, as discussed by Borg et al. [43], suggest that the presence of recycled fines alters the hydration balance by introducing phases with higher porosity and water retention capacity, while also carrying pre-carbonated material that contributes to additional mass loss at high temperature. The increased CH and carbonate signals point to a less efficient pozzolanic consumption of portlandite and a higher susceptibility to carbonation, which may limit the ability of recycled fines to actively contribute to strength development. Taken together with the observed performance reduction, these findings highlight that the underperformance of recycled fines cannot be ascribed solely to water absorption, but also to their influence on microstructure and phase assemblage.

5. Life cycle assessment

The Life Cycle Assessment (LCA) was conducted according to the ISO 14040:2006 and ISO 14044:2006 [74,75], and structured as follows: goal and scope definition, inventory analysis, Life Cycle Impact Assessment (LCIA), interpretation and discussion of the results.

5.1. Goal and scope

As discussed in the previous sections, recycling Ultra-High Performance Concrete (UHPC) has proven to be a technically feasible approach for producing new UHPC with potential environmental benefits. However, the recycling process entails significant

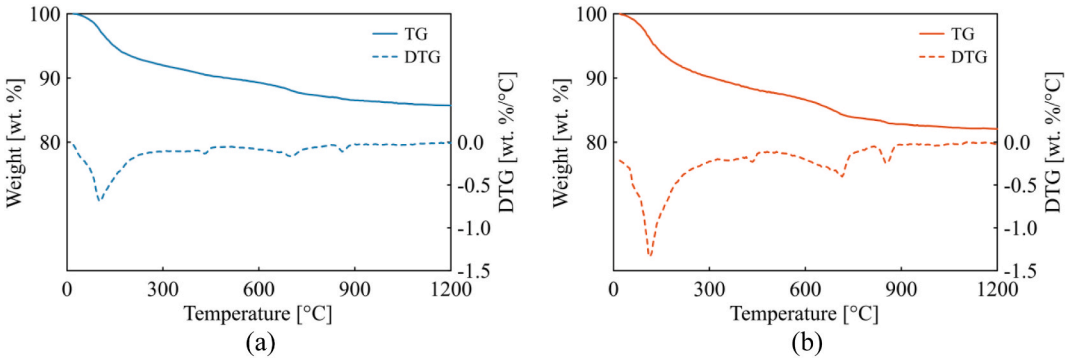

Fig. 17. Thermogravimetric-differential thermal analysis on samples before the damage and curing periods; (a) reference mix (REF), and (b) mix with aggregates and cement replacement (C100F).

environmental burdens, primarily due to machinery operation and the consequent energy consumption. These burdens may risk offsetting the environmental benefits gained from substituting virgin materials, given the intensive efforts required to obtain useable recycled fractions. Consequently, a broader assessment of the environmental trade-offs is necessary to support informed decision-making.

The goal of this study was to conduct a comparative environmental assessment of UHPC incorporating different recycled UHPC fractions. Two recycling scenarios were analysed, corresponding to the mixes C100C and C100F, in which all the natural aggregates used in the reference mix (REF) are replaced with crushed UHPC, and 30 % of the cement content is substituted with additional recycled fractions. In the C100C mix, the recycled material was used in accordance with the required granulometry, while C100F incorporated an additional fraction of fine particles.

In the environmental assessment of structural materials, the selection of the functional unit (FU) is crucial, as it must reflect mechanical performance. In this study, a functional unit of one cubic meter (1 m^3) of UHPC or R-UHPC was adopted. To account for the material mechanical efficiency, the results were further normalized based on long-term compressive strength and long-term flexural strength. Both normalized results are expressed for 1 m^3/MPa, with the corresponding strength values used for normalization detailed in Table 2.

This study was conducted within a cradle-to-gate system boundary, as illustrated in Fig. 18. In accordance with the cut-off approach, recycled UHPC aggregates were treated as burden-free at the point of generation, in line with previous studies [76]. The demolition of the original structure was assumed to occur independently of the present system and was therefore excluded from the analysis. Only the environmental impacts associated with the transport, additional crushing, sieving of recycled materials, and transport of wastes and recycled steel fibres were considered, as already proposed in Ref. [29].

In the baseline case, the raw materials required for UHPC production are produced and delivered to the batching plant (100–262 km, depending on the material). In the two recycling scenarios (C100C and C100F), the UHPC chunks resulting from the demolition of an old UHPC structure are transported to the batching plant (100 km), where they are processed using a custom-built on-site UHPC recycling machine (details provided in Refs. [77,78]). After processing and sieving, coarser particles not suitable for reuse are kept in the same facility, while other minor wastes resulting from the process (plastic, wood) and extracted steel fibres are transferred to a recycling plant (92.9 km). Finer fractions are utilized in the production of C100C and C100F, fully replacing natural aggregates and partially substituting cement, thereby reducing the need for virgin material extraction, processing, and transportation.

It should be noted that the particle size distribution produced by the recycling equipment does not perfectly match the specification required for UHPC production, as detailed in Ref. [79]. As a result, the input quantity of UHPC chunks exceeds 1 m^3 to meet the precise fine fraction demand for the C100C (1.48 m^3) and C100F mixes (1.64 m^3).

Finally, the steel fibres recovered during the recycling process are sent to an external facility. Although this study has demonstrated the technical feasibility of using these recycled fibres as a complete substitute for virgin steel fibres, the combined use of recycled fibres, aggregates, and partial cement replacement has yet to be explored in practice.

5.2. Life cycle impact assessment

The life cycle impact assessment (LCIA) phase was conducted using the CML-IA baseline method, implemented within the SimaPro® software environment and relying on secondary data from the Ecoinvent database (version 3.10). Only the environmental impacts associated with the on-site recycling machine were derived from primary data. The CML-IA method provides midpoint indicators, which represent environmental impacts at an intermediate stage of the cause–effect chain.

Ten impact categories were selected based on their relevance and widespread application in the environmental assessment of construction materials. These include: Abiotic Depletion (ADP), Global Warming Potential (GWP100a), Ozone Layer Depletion Potential (ODP), Human Toxicity Potential (HTP), Freshwater Aquatic Ecotoxicity (FAETP), Marine Aquatic Ecotoxicity (MAETP), Terrestrial Ecotoxicity (TETP), Photochemical Oxidation Potential (POCP), Acidification Potential (AP), and Eutrophication Potential (EP).

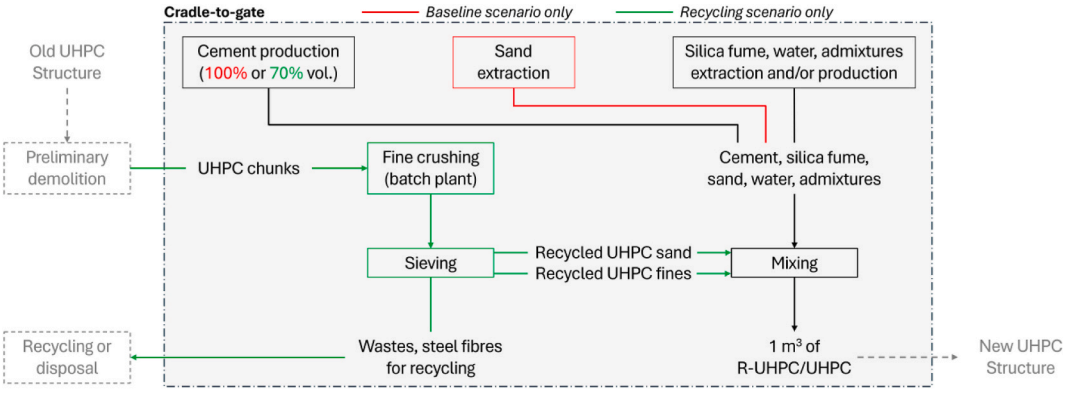

Fig. 18. Flow diagram and system boundaries of the LCA study.

All results are expressed relative to the functional unit defined in this study – 1 m^3 of UHPC or R-UHPC – to enable a consistent comparison of environmental performance across the different mix scenarios.

5.3. Results

The results of the midpoint impact assessment are presented in Table 3. When using a functional unit of 1 m^3, the mix with graded aggregates only (C100C) exhibits lower or comparable impacts relative to the baseline scenario (REF). In contrast, the mix containing additional fines (C100F) shows slightly higher impacts in a few categories, primarily due to a different breakdown of contributions. Fig. 19 illustrates the contribution of each inventory item to the impact categories, normalized against the total impact of each category for the reference mix – hence, the stacked bars for REF always sum to 100 %. The graph highlights that, although energy is required for crushing during the recycling process, its share of the total impacts is negligible compared to other key contributors, particularly the production of cement, steel fibres, and additives. Consequently, the reduced cement content in the recycled mixes offsets the additional burdens in most cases. However, this beneficial effect is partially offset by the transportation of UHPC chunks from the original structure to the recycling and batching plant.

Further insights are provided in Figs. 20 and 21, where results are normalized based on compressive and flexural strength, respectively. This normalization highlights the importance of accounting for mechanical performance when comparing environmental impacts, as mixes with higher strength can deliver the same structural function using less material. By incorporating strength-based normalization, the assessment enables a more equitable and functionally relevant comparison among the different mix designs. Since the CML-IA midpoint categories are expressed in different units, all impact values are scaled relative to the baseline scenario (REF), which is set at 100 %.

Two principal conclusions can be drawn from this further analysis. First, the normalization parameter significantly influences the outcome of the LCIA. When compressive strength is used, both R-UHPC mixes benefit from the substantial long-term strength gains, leading to improved environmental performance across most indicators. In contrast, when normalized by flexural strength, the environmental impacts of the R-UHPC mixes increase across all categories, irrespective of the mix design. The sole exception is the GWP100a value for mix C100C (produced with unsorted recycled aggregates), which demonstrates a marked reduction due to its reduced clinker production volume – clinker being the primary contributor to CO_2-equivalent emissions in UHPC production.

Second, the C100F mix, incorporating an additional fraction of recycled fines, consistently exhibits higher environmental impacts across all midpoint categories. This increase is attributed to the combined effect of the elevated energy demand associated with fine particle recovery and processing, and the greater volume of UHPC chunks required for C100F (1.64 m^3 per 1 m^3 of mix) compared to C100C (1.48 m^3 per 1 m^3), which intensifies the impact of transportation and offsets the material substitution benefits observed in C100C.

Overall, the balance between the environmental advantages of recycled UHPC – primarily stemming from reduced extraction and processing of virgin raw materials – and the burdens introduced by energy-intensive recycling operations, is highly dependent on the mechanical performance metric used. This dependency underscores the importance of functional performance-based normalization when evaluating sustainable alternatives for structural concretes.

5.4. Thoroughgoing Sustainability Index

An alternative perspective on the sustainability performance of recycled UHPC can be obtained using the Thoroughgoing Sustainability Index (TS), as proposed by di Summa et al. [80]. In particular, the material index (TS,M) offers a concise measure of the environmental efficiency of 1 m^3 of material relative to a baseline scenario. This index is defined as the ratio between selected material performance properties and CML impact indicators, both normalized against the reference case. For UHPC, the two performance properties considered were long-term compressive strength and flexural strength (Eq. (7)), consistent with the normalization parameters used in the previous section.

$$\mathrm{TS,M} = \frac{\left(\frac{f_c}{f_{c,REF}} + \frac{f_{fl}}{f_{fl,REF}}\right) \Big/ 2}{\left(\sum_{i=1}^{10} \frac{CML_i}{CML_{i,REF}}\right) \Big/ 10} \tag{7}$$

when the TS,M index exceeds 1, the material under investigation is considered more efficient than the reference (REF), due to superior mechanical performance, reduced environmental impacts, or a combination of both.

To further account for the self-healing capabilities of the mixes, the TS,M index can be extended by incorporating normalized healing indices into the numerator. In this study, two parameters were included: the Index of Crack Sealing (ICS_0) and the Index of Sorptivity Healing (ISH_0), both evaluated after six months of exposure. These parameters were selected as they represent the most relevant indicators of UHPC durability enhancement through autogenous healing, which contributes significantly to the preservation of long-term performance. The resulting material index (TS,M*) is presented in Eq. (8).

Table 3
Results of the Life Cycle Impact Assessment for the three cases.

Impact category	Unit	REF	C100C	C100F
Abiotic depletion (ADP)	kg Sb-eq.	4.42×10^{-3}	4.34×10^{-3}	4.37×10^{-3}
Global warming (GWP100a)	kg CO_2-eq.	1160.2	956.3	964.1
Ozone layer depletion (ODP)	kg CFC-11-eq.	8.31×10^{-6}	8.34×10^{-6}	8.45×10^{-6}
Human toxicity (HTP)	kg 1,4-DB-eq.	2.415×10^{4}	2.415×10^{4}	2.418×10^{4}
Fresh water aquatic ecotoxicity (FAETP)	kg 1,4-DB-eq.	2.637×10^{3}	2.621×10^{3}	2.625×10^{3}
Marine aquatic ecotoxicity (MAETP)	kg 1,4-DB-eq.	8.718×10^{6}	8.680×10^{6}	8.691×10^{6}
Terrestrial ecotoxicity (TETP)	kg 1,4-DB-eq.	150.03	149.87	150.06
Photochemical oxidation (POCP)	kg C_2H_4-eq.	0.235	0.221	0.222
Acidification (AP)	kg SO_2-eq.	3.200	2.819	2.844
Eutrophication (EP)	kg PO_4^{3-}-eq.	1.272	1.149	1.155

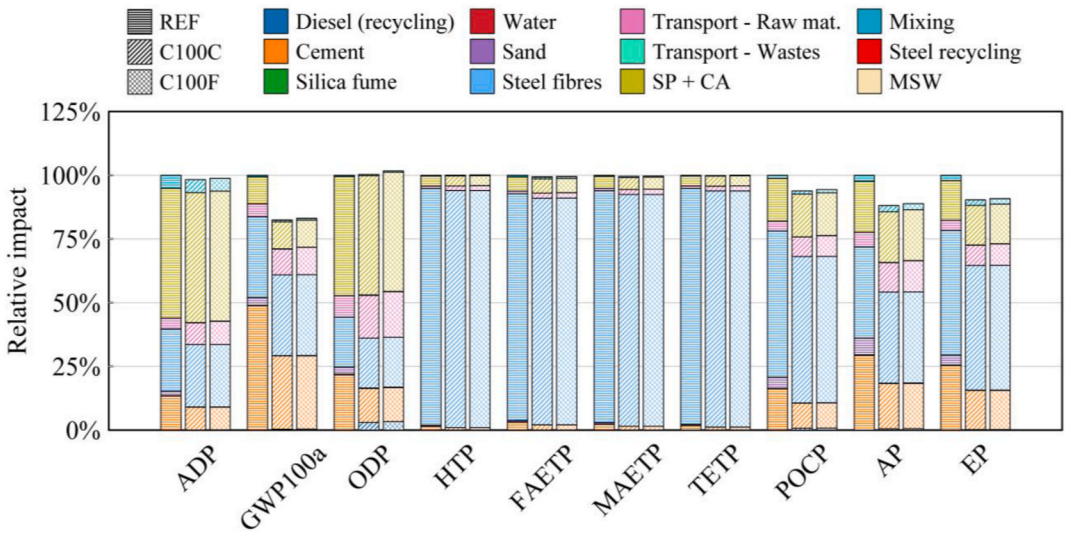

Fig. 19. Breakdown of contributions to each impact category, with impacts normalized to the total value of the reference scenario (REF) in each category.

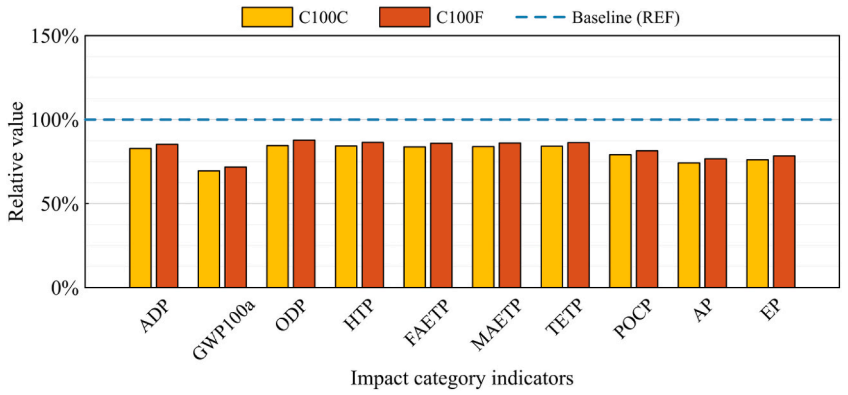

Fig. 20. Relative values of the impact category indicators for the two recycling scenarios with respect to the baseline; the functional unit is 1 m^3/MPa of compressive strength.

$$\mathrm{TS,M}^{*} = \frac{\left(\frac{f_c}{f_{c,REF}} + \frac{f_{fl}}{f_{fl,REF}} + \frac{{ICS_0}^{6m}}{{ICS_{0,REF}}^{6m}} + \frac{{ISH_0}^{6m}}{{ISH_{0,REF}}^{6m}}\right) \Big/ 4}{\left(\sum_{i=1}^{10} \frac{CML_i}{CML_{i,REF}}\right) \Big/ 10} \tag{8}$$

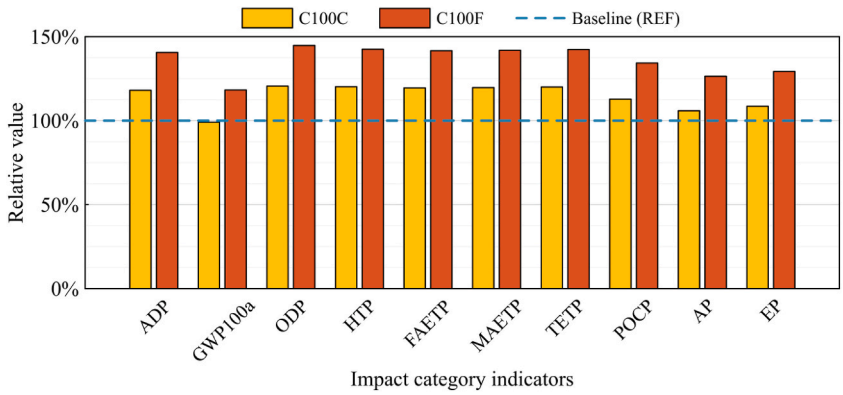

Fig. 21. Relative values of the impact category indicators for the two recycling scenarios with respect to the baseline; the functional unit is 1 m^3/MPa of flexural strength.

Table 4 presents the values of both indices for the two R-UHPC mixes. The mix incorporating unsorted fines (C100C) yields TS,M and TS,M* values greater than 1, underscoring its improved sustainability performance relative to the reference. This outcome reflects the combined effect of reduced environmental impacts and significantly enhanced compressive strength, with the drawback of lower flexural strength only partially diminishing its overall efficiency. The advantage becomes even more pronounced when self-healing performance is considered in the TS,M* index, owing to the mix superior autogenous healing capacity.

In contrast, the mix with additional sorted fines (C100F) exhibits generally inferior performance. While it achieves slightly reduced environmental impacts in select categories and maintains a comparable compressive strength, these benefits are offset by weaker flexural performance and diminished self-healing capacity, resulting in lower overall index values.

6. Conclusions

This study has evaluated the self-healing performance of two recycled Ultra-High Performance Concrete (R-UHPC) mixes, developed from a parent UHPC mix by completely replacing aggregates and partially substituting cement with either unsorted recycled aggregates or recycled fines. This research represents the final phase of a four-year initiative aimed at significantly reducing the embodied carbon of UHPC and mitigating resource depletion from raw material extraction.

A comprehensive multi-parameter approach was employed to investigate, together with the mechanical performance, the evolution of the durability and of the autogenous self-healing capability over time, also correlated with microscopic-scale visual observations. Pre-cracked and repeatedly damaged specimens underwent different curing periods in a 3.3 % NaCl solution, alternated with experimental characterization at 1, 2, 3, and 6 months. The healing performance was compared against previous results from mixes where only aggregates, and not cement, were replaced. Long-term (3 years) performance data were also provided to compare the two newly developed mixes with those investigated in previous studies.

In parallel, a cradle-to-gate life cycle assessment was conducted to evaluate the environmental performance of the R-UHPC mixes, with particular attention to the influence of mechanical performance differences. By integrating functional performance into the LCA through normalization over compressive and flexural strength, the study provides a more meaningful comparison of the environmental impacts, ensuring that sustainability assessments are directly aligned with structural functionality.

The experimental campaign yielded the following outcomes.

- Up to 30 % of the Portland cement content in UHPC could be successfully replaced with recycled UHPC without compromising mechanical and durability performance, as results were largely comparable to reference mixes; the strength development was guaranteed by the significant presence of unhydrated cement particles in the recycled material.
- Both R-UHPC mixes (C100C with recycled unsorted aggregates and C100F with recycled fines) exhibited the characteristic self-healing capacity of UHPC, consistently sealing induced cracks.
- In pre-cracked specimens, the cracks were entirely sealed, and most recovery was observed within the first two months. In specimens subjected to repeated cracking-healing cycles, the closure rate exceeded 40 % in all cases.
- Crack closure reduced sorptivity (−70 % when pre-cracked, up to −50 % when repeatedly cracked) and increased stiffness (up to +20 % in both cases), although repeated damage progressively diminished the residual healing capacity.

Table 4
Thoroughgoing Sustainability Index for the two R-UHPC mixes.

Mix	TS,M	TS,M*
C100C	1.060	1.223
C100F	0.972	0.968

- The mix with recycled fines (C100F) demonstrated reduced healing efficiency due to the inherently high water absorption of the fine recycled particles, negatively impacting sorptivity.
- The flexural response and fracture behaviour of specimens highlighted the role of healing products in preserving strength and stiffness; enhanced fibre-matrix interaction resulting from the healing process contributed to constant mechanical performance.
- The choice of functional unit based on mechanical performance significantly influences the environmental assessment, as normalization over compressive strength favours the R-UHPC mixes, while normalization over flexural strength results in higher relative impacts, highlighting the importance of performance-based comparisons in structural applications; however, when the more comprehensive TS index was adopted, the mix with unsorted recycled fines demonstrated a superior efficiency with respect to the reference.
- The inclusion of additional fine recycled fractions increases environmental burdens, primarily due to the additional processing as well as to the transportation of UHPC chunks to a new construction site, which might offset the benefits of raw material substitution.

This study provided a preliminary yet extensive validation of a recycling strategy that incorporates various fractions of crushed UHPC to produce new R-UHPC. The recycled mixes preserved the unique properties of the parent material, demonstrating potential for sustainable UHPC production. However, the finer fraction presents challenges due to its high water absorption, which may impair durability, particularly in aggressive environments. The life cycle assessment further highlighted the environmental trade-offs of using such recycled fractions, especially when additional processing is required. Future work should address these limitations by advancing efficient recycling facilities, fostering a more distributed industry to reduce transport distances, and optimizing mix designs through alternative processing, surface treatments, or tailored particle size distributions. In addition, longer exposure times should be considered to better assess the long-term durability of this class of materials, thereby ensuring robust mechanical and environmental performance across diverse applications. In parallel, closer collaboration with industry stakeholders and the development of pilot projects will be essential to validate the technical and economic feasibility of R-UHPC in real-world applications and to support the establishment of standards ensuring its reliable large-scale deployment.

CRediT authorship contribution statement

Marco Davolio: Writing – review & editing, Writing – original draft, Visualization, Methodology, Investigation, Formal analysis, Data curation, Conceptualization. **Estefania Cuenca:** Writing – review & editing, Validation, Supervision, Methodology, Conceptualization. **Davide di Summa:** Writing – review & editing, Software, Methodology, Formal analysis. **Ruben Paul Borg:** Writing – review & editing, Project administration, Funding acquisition, Conceptualization. **Liberato Ferrara:** Writing – review & editing, Validation, Supervision, Resources, Project administration, Methodology, Funding acquisition, Conceptualization.

Declaration of competing interest

The authors declare that they have no known competing financial interests or personal relationships that could have appeared to influence the work reported in this paper.

Acknowledgements

The present work represents the sequel of a research line started in the framework of the Horizon 2020 ReSHEALience project (GA 760824), completed in 2022, which found its continuation in the activity of Task 4.4 of Horizon Europe SINCERE project, The second life of modern period architecture: Resilient and adaptive renovation towards net-zero carbon heritage buildings (GA 101123293) whose support is gratefully acknowledged.

Data availability

Data will be made available on request.

References

[1] United States Geological Survey, Mineral Commodity Summaries 2024, 2024.
[2] K. Kabirifar, M. Mojtahedi, C. Wang, V.W.Y. Tam, Construction and demolition waste management contributing factors coupled with reduce, reuse, and recycle strategies for effective waste management: a review, J. Clean. Prod. 263 (2020), https://doi.org/10.1016/j.jclepro.2020.121265.
[3] A. Damgaard, C. Lodato, S. Butera, T.A. Fruergaard, M. Kamps, L. Corbin, D. Tonini, T.F. Astrup, Background data collection and life cycle assessment for construction and demolition waste (CDW) management. https://doi.org/10.2760/772724, 2022.
[4] European Parliament, European Council, DIRECTIVE 2008/98/EC on Waste and Repealing Certain Directives, 2008.
[5] Q. Wang, Y. Zhao, L. Sun, H. Zheng, X. Liang, Exploring economic and environmental impacts of recycled aggregate concrete using particle swarm optimization algorithm, J. Clean. Prod. 475 (2024), https://doi.org/10.1016/j.jclepro.2024.143713.
[6] K.P. Verian, W. Ashraf, Y. Cao, Properties of recycled concrete aggregate and their influence in new concrete production, Resour. Conserv. Recycl. 133 (2018) 30–49, https://doi.org/10.1016/j.resconrec.2018.02.005.
[7] S.C. Kou, C.S. Poon, M. Etxeberria, Influence of recycled aggregates on long term mechanical properties and pore size distribution of concrete, Cem. Concr. Compos. 33 (2011) 286–291, https://doi.org/10.1016/j.cemconcomp.2010.10.003.

[8] M.J. McGinnis, M. Davis, A. de la Rosa, B.D. Weldon, Y.C. Kurama, Strength and stiffness of concrete with recycled concrete aggregates, Constr. Build. Mater. 154 (2017) 258–269, https://doi.org/10.1016/j.conbuildmat.2017.07.015.
[9] C. Thomas, J. Setién, J.A. Polanco, P. Alaejos, M. Sánchez De Juan, Durability of recycled aggregate concrete, Constr. Build. Mater. 40 (2013) 1054–1065, https://doi.org/10.1016/j.conbuildmat.2012.11.106.
[10] P. Saravanakumar, K. Abhiram, B. Manoj, Properties of treated recycled aggregates and its influence on concrete strength characteristics, Constr. Build. Mater. 111 (2016) 611–617, https://doi.org/10.1016/j.conbuildmat.2016.02.064.
[11] Y. Liang, Z. Ye, F. Vernerey, Y. Xi, Development of processing methods to improve strength of concrete with 100% recycled coarse aggregate, J. Mater. Civ. Eng. 27 (2015), https://doi.org/10.1061/(asce)mt.1943-5533.0000909.
[12] J. Xiao, H. Zhang, Y. Tang, Q. Deng, D. Wang, C. sun Poon, Fully utilizing carbonated recycled aggregates in concrete: strength, drying shrinkage and carbon emissions analysis, J. Clean. Prod. 377 (2022), https://doi.org/10.1016/j.jclepro.2022.134520.
[13] Y. Dong, Performance assessment and design of ultra-high performance concrete (UHPC) structures incorporating life-cycle cost and environmental impacts, Constr. Build. Mater. 167 (2018) 414–425, https://doi.org/10.1016/j.conbuildmat.2018.02.037.
[14] C. Magureanu, I. Sosa, C. Negrutiu, B. Heghes, Mechanical properties and durability of ultra-high-performance concrete, ACI Mater. J. 109 (2012) 177–184.
[15] J. Li, Z. Wu, C. Shi, Q. Yuan, Z. Zhang, Durability of ultra-high performance concrete – a review, Constr. Build. Mater. 255 (2020) 1–13, https://doi.org/10.1016/j.conbuildmat.2020.119296.
[16] Z. Li, H. Zhang, R. Wang, Influence of steel fiber distribution on splitting damage and transport properties of ultra-high performance concrete, Cem. Concr. Compos. 126 (2022) 1–15, https://doi.org/10.1016/j.cemconcomp.2021.104373.
[17] E.G. Moffatt, M.D.A. Thomas, A. Fahim, R.D. Moser, Performance of ultra-high-performance Concrete in harsh marine environment for 21 years, ACI Mater. J. 117 (2020) 105–112, https://doi.org/10.14359/51727022.
[18] M. Li, V.C. Li, Cracking and healing of engineered cementitious composites under Chloride environment, ACI Mater. J. 108 (2011) 333–340.
[19] S. Zhao, L. Jiang, H. Chu, A preliminary investigation of energy consumption in fracture of ultra-high performance concrete, Constr. Build. Mater. 237 (2020) 1–12, https://doi.org/10.1016/j.conbuildmat.2019.117634.
[20] F. Lo Monte, L. Ferrara, Self-healing characterization of UHPFRCC with crystalline admixture: experimental assessment via multi-test/multi-parameter approach, Constr. Build. Mater. 283 (2021) 1–12, https://doi.org/10.1016/j.conbuildmat.2021.122579.
[21] E. Cuenca, M. Criado, M. Giménez, M.C. Alonso, L. Ferrara, Effects of Alumina nanofibers and cellulose nanocrystals on durability and self-healing capacity of ultrahigh-performance fiber-reinforced concretes, J. Mater. Civ. Eng. 34 (2022) 1–17, https://doi.org/10.1061/(asce)mt.1943-5533.0004375.
[22] D. di Summa, M. Parpanesi, L. Ferrara, N. De Belie, A holistic life cycle design approach to enhance the sustainability of concrete structures, Struct. Concr. 24 (2023) 7684–7704, https://doi.org/10.1002/suco.202300645.
[23] S. Al-Obaidi, P. Bamonte, F. Animato, F. Lo Monte, I. Mazzantini, M. Luchini, S. Scalari, L. Ferrara, Innovative design concept of cooling water tanks/basins in geothermal power plants using ultra-high-performance Fiber-Reinforced Concrete with enhanced durability, Sustainability 13 (2021) 1–26, https://doi.org/10.3390/su13179826.
[24] S. Al Obaidi, M. Davolio, F. Lo Monte, F. Costanzi, M. Luchini, P. Bamonte, L. Ferrara, Structural validation of geothermal water basins constructed with durability enhanced Ultra High Performance Fiber Reinforced Concrete (Ultra High Durability Concrete), Case Stud. Constr. Mater. 17 (2022) 1–24, https://doi.org/10.1016/j.cscm.2022.e01202.
[25] I. Lande, R. Terje Thorstensen, Comprehensive sustainability strategy for the emerging ultra-high-performance concrete (UHPC) industry, Cleaner Materials 8 (2023), https://doi.org/10.1016/j.clema.2023.100183.
[26] H.M. Hamada, J. Shi, F. Abed, M.S. Al Jawahery, A. Majdi, S.T. Yousif, Recycling solid waste to produce eco-friendly ultra-high performance concrete: a review of durability, microstructure and environment characteristics, Sci. Total Environ. 876 (2023), https://doi.org/10.1016/j.scitotenv.2023.162804.
[27] P. Wu, K. Dai, Y. Shi, H. Rong, X. Zhang, Effect of biomass ash on hydration, properties and microstructure of ultra-high performance concrete, J. Build. Eng. 104 (2025) 112276, https://doi.org/10.1016/j.jobe.2025.112276.
[28] S. Ahmed, A. Rehman, A. Amjad, M.H. Hasib, F. Hussain, A.Q. Khan, R.A. Khushnood, Development of multifunctional cementitious composite using biochar, J. Build. Eng. 96 (2024) 110598, https://doi.org/10.1016/j.jobe.2024.110598.
[29] N.P. Kannikachalam, D. di Summa, R.P. Borg, E. Cuenca, M. Parpanesi, N. De Belie, L. Ferrara, Assessment of sustainability and self-healing performances of recycled ultra-high-performance concrete, ACI Mater. J. 120 (2023) 117–132, https://doi.org/10.14359/51737336.
[30] E. Brühwiler, E. Denarié, Rehabilitation and strengthening of concrete structures using ultra-high performance fibre reinforced concrete, Struct. Eng. Int.: Journal of the International Association for Bridge and Structural Engineering (IABSE) 23 (2013) 450–457, https://doi.org/10.2749/101686613X13627347100437.
[31] N.M. Azmee, N. Shafiq, Ultra-high performance concrete: from fundamental to applications, Case Stud. Constr. Mater. 9 (2018), https://doi.org/10.1016/j.cscm.2018.e00197.
[32] J. Abellán-García, J.S. Carvajal-Muñoz, C. Ramírez-Munévar, Application of ultra-high-performance concrete as bridge pavement overlays: literature review and case studies, Constr. Build. Mater. 410 (2024), https://doi.org/10.1016/j.conbuildmat.2023.134221.
[33] K. Chen, S. Cheng, Q. Wu, X. Chen, C. Zhao, S. Li, J. Lu, Utilization of recycled fine aggregate in ultra-high performance concrete: mechanical strength, microstructure and environment impacts, Constr. Build. Mater. 439 (2024), https://doi.org/10.1016/j.conbuildmat.2024.137364.
[34] Q.H. Li, S.Y. Zhao, B.T. Huang, L.Y. Xu, S.L. Xu, Simultaneous enhancement of ductility and sustainability of high-strength Strain-Hardening Cementitious Composites (SHCC) using recycled fine aggregates, J. Clean. Prod. 470 (2024), https://doi.org/10.1016/j.jclepro.2024.143357.
[35] L. Luo, M. Jia, X. Cheng, Experimental study and analytical modeling of tensile performance of ultra-high-performance concrete incorporating modified recycled aggregates, J. Clean. Prod. 468 (2024), https://doi.org/10.1016/j.jclepro.2024.143123.
[36] L. Luo, J. Shi, J. Wang, Y. Qu, B. Dai, Experimental study on flexural performance of ultra-high-performance concrete with recycled aggregate co-modified by nano-silica and steel fiber, Constr. Build. Mater. 411 (2024), https://doi.org/10.1016/j.conbuildmat.2023.134417.
[37] C. Yuan, L. Yong, C. Ziao, Y. Tianyi, Y. Rui, Development of Ultra-High Performance Concrete (UHPC) matrix based on recycled concrete fines subjected to coupling curing of microwave and wet carbonation, J. Build. Eng. 95 (2024), https://doi.org/10.1016/j.jobe.2024.110038.
[38] H. Wu, C. Liu, Y. Zhao, G. Chen, J. Gao, Elucidating the role of recycled concrete powder in low-carbon ultra-high performance concrete (UHPC): Multi-performance evaluation, Constr. Build. Mater. 441 (2024), https://doi.org/10.1016/j.conbuildmat.2024.137520.
[39] L. De Brabandere, V. Grigorjev, P. Van den Heede, H. Nachtergaele, K. Degezelle, N. De Belie, Using fines from recycled high-quality concrete as a substitute for cement, Sustainability 17 (2025) 1506, https://doi.org/10.3390/su17041506.
[40] M. Rajczakowska, L. Nilsson, K. Habermehl-Cwirzen, H. Hedlund, A. Cwirzen, Does a high amount of unhydrated Portland cement ensure an effective autogenous self-healing of mortar? Materials 12 (2019) https://doi.org/10.3390/ma12203298.
[41] D. Qian, R. Yu, Z. Shui, Y. Sun, C. Jiang, F. Zhou, M. Ding, X. Tong, Y. He, A novel development of green ultra-high performance concrete (UHPC) based on appropriate application of recycled cementitious material, J. Clean. Prod. 261 (2020), https://doi.org/10.1016/j.jclepro.2020.121231.
[42] S. Medjigbodo, A.Z. Bendimerad, E. Rozière, A. Loukili, How do recycled concrete aggregates modify the shrinkage and self-healing properties? Cem. Concr. Compos. 86 (2018) 72–86, https://doi.org/10.1016/j.cemconcomp.2017.11.003.
[43] R.P. Borg, E. Cuenca, R. Garofalo, F. Schillani, M.L. Nasner, L. Ferrara, Performance assessment of Ultra-High Durability Concrete produced from recycled Ultra-High Durability Concrete, Front Built Environ 7 (2021), https://doi.org/10.3389/fbuil.2021.648220.
[44] P. Serna, F. Lo Monte, E.J. Mezquida-Alcaraz, E. Cuenca, V. Mechtcherine, M. Reichardt, A. Peled, O. Regev, R.P. Borg, A. Tretjakov, D. Lizunov, K. Sobolev, S. Sideri, K. Nelson, E.M. Gastaldo Brac, L. Ferrara, Upgrading the Concept of UHPFRC for High Durability in the Cracked State: the Concept of Ultra High Durability Concrete (UHDC) in the Approach of the H2020 Project Reshealience, 2019. Dennis Lizunov.
[45] H. Kang, J. Moon, Secondary curing effect on the hydration of ultra-high performance concrete, Constr. Build. Mater. 298 (2021), https://doi.org/10.1016/j.conbuildmat.2021.123874.

[46] L. Ferrara, R.P. Borg, E. Cuenca, M. El-Sayed, C. Vassallo, Recycled Ultra High Performance Concrete (UHPC) as a way to reduce the cement demand in new UHPC, in: Building for the Future: Durable, Sustainable, Resilient, 2023, pp. 486–495.
[47] M. Davolio, E. Cuenca, R.P. Borg, L. Ferrara, Self-healing performance of recycled UHPC under chloride exposure, in: L. Ferrara, G. Muciaccia, D. di Summa (Eds.), Proceedings of the RILEM Spring Convention and Conference 2024, Springer, 2025, pp. 82–90, https://doi.org/10.1007/978-3-031-70281-5_10.
[48] European Committee for Standardization, EN 196-6 - Methods of Testing Cement - Part 6, Determination of fineness, 2019.
[49] L. Berredjem, N. Arabi, L. Molez, Mechanical and durability properties of concrete based on recycled coarse and fine aggregates produced from demolished concrete, Constr. Build. Mater. 246 (2020), https://doi.org/10.1016/j.conbuildmat.2020.118421.
[50] P. Belin, G. Habert, M. Thiery, N. Roussel, Cement paste content and water absorption of recycled concrete coarse aggregates, Materials and Structures/Materiaux et Constructions 47 (2014) 1451–1465, https://doi.org/10.1617/s11527-013-0128-z.
[51] J. Bao, S. Li, P. Zhang, X. Ding, S. Xue, Y. Cui, T. Zhao, Influence of the incorporation of recycled coarse aggregate on water absorption and chloride penetration into concrete, Constr. Build. Mater. 239 (2020), https://doi.org/10.1016/j.conbuildmat.2019.117845.
[52] European Committee for Standardization, EN 1015-11 - Methods of Test for Mortar for Masonry - Part 11: Determination of Flexural and Compressive Strength of Hardened Mortar, 2019, 15.
[53] ASTM International, Astm C1585-20 - Standard Test method for measurement of rate of absorption of water by hydraulic-cement concretes. https://doi.org/10.1520/C1585-20, 2020.
[54] E. Cuenca, A. Mezzena, L. Ferrara, Synergy between crystalline admixtures and nano-constituents in enhancing autogenous healing capacity of cementitious composites under cracking and healing cycles in aggressive waters, Constr. Build. Mater. 266 (2021), https://doi.org/10.1016/j.conbuildmat.2020.121447.
[55] B. Xi, L. Ferrara, Evolution of self-healing performance of UHPC exposed to aggressive environments and cracking/healing cycles, Materials and Structures/Materiaux et Constructions 57 (2024), https://doi.org/10.1617/s11527-024-02312-2.
[56] Z. Duan, Z. Lv, J. Xiao, C. Liu, X. Nong, Study on the performance of recycled coarse and fine aggregates as microbial carriers applied to self-healing concrete, Materials 16 (2023), https://doi.org/10.3390/ma16062371.
[57] M. Luo, A. Ji, X. Li, D. Yang, Performance evaluation of self-healing recycled concrete using biomineralization modified recycled aggregate as bacterial carrier, J. Build. Eng. 86 (2024), https://doi.org/10.1016/j.jobe.2024.109000.
[58] V. Cappellesso, D. di Summa, P. Pourhaji, N. Prabhu Kannikachalam, K. Dabral, L. Ferrara, M. Cruz Alonso, E. Camacho, E. Gruyaert, N. De Belie, A review of the efficiency of self-healing concrete technologies for durable and sustainable concrete under realistic conditions, Int. Mater. Rev. 68 (2023) 556–603, https://doi.org/10.1080/09506608.2022.2145747.
[59] H. Doostkami, M. Roig-Flores, P. Serna, Self-healing efficiency of Ultra High-Performance Fiber-Reinforced Concrete through permeability to chlorides, Constr. Build. Mater. 310 (2021), https://doi.org/10.1016/j.conbuildmat.2021.125168.
[60] A. Akhavan, S.M.H. Shafaatian, F. Rajabipour, Quantifying the effects of crack width, tortuosity, and roughness on water permeability of cracked mortars, Cement Concr. Res. 42 (2012) 313–320, https://doi.org/10.1016/j.cemconres.2011.10.002.
[61] S. Hou, K. Li, Z. Wu, F. Li, C. Shi, Quantitative evaluation on self-healing capacity of cracked concrete by water permeability test – a review, Cem. Concr. Compos. 127 (2022), https://doi.org/10.1016/j.cemconcomp.2021.104404.
[62] K. Kaptan, S. Cunha, J. Aguiar, A review of the utilization of recycled powder from concrete waste as a cement partial replacement in cement-based materials: fundamental properties and activation methods, Applied Sciences (Switzerland) 14 (2024), https://doi.org/10.3390/app14219775.
[63] L. Evangelista, J. de Brito, Mechanical behaviour of concrete made with fine recycled concrete aggregates, Cem. Concr. Compos. 29 (2007) 397–401, https://doi.org/10.1016/j.cemconcomp.2006.12.004.
[64] C. Vintimilla, M. Etxeberria, Limiting the maximum fine and coarse recycled aggregates-type a used in structural concrete, Constr. Build. Mater. 380 (2023), https://doi.org/10.1016/j.conbuildmat.2023.131273.
[65] M. Davolio, S. Al-Obaidi, M.Y. Altomare, F. Lo Monte, L. Ferrara, A methodology to assess the evolution of mechanical performance of UHPC as affected by autogenous healing under sustained loadings and aggressive exposure conditions, Cem. Concr. Compos. 139 (2023). https://doi.org/10.1016/j.cemconcomp.2023.105058.
[66] M. Alameri, M.S. Mohamed Ali, M. Elchalakani, A. Sheikh, R. Fan, Self-Healing and mechanical behaviour of fibre-reinforced ultra-high-performance concrete incorporating superabsorbent polymer under repeated and sustained loadings, Fibers 12 (2024), https://doi.org/10.3390/fib12110095.
[67] Y. Liu, P. Ren, N. Garcia-Troncoso, K.H. Mo, T.C. Ling, Roles of enhanced ITZ in improving the mechanical properties of concrete prepared with different types of recycled aggregates, J. Build. Eng. 60 (2022), https://doi.org/10.1016/j.jobe.2022.105197.
[68] S. Al-Obaidi, S. He, E. Schlangen, L. Ferrara, Effect of matrix self-healing on the bond-slip behavior of micro steel fibers in ultra-high-performance concrete, Materials and Structures/Materiaux et Constructions 56 (2023), https://doi.org/10.1617/s11527-023-02250-5.
[69] V. Marcos-Meson, A. Solgaard, G. Fischer, C. Edvardsen, A. Michel, Pull-out behaviour of hooked-end steel fibres in cracked concrete exposed to wet-dry cycles of chlorides and carbon dioxide – mechanical performance, Constr. Build. Mater. 240 (2020), https://doi.org/10.1016/j.conbuildmat.2019.117764.
[70] S. Pyo, T. Koh, M. Tafesse, H.K. Kim, Chloride-induced corrosion of steel fiber near the surface of ultra-high performance concrete and its effect on flexural behavior with various thickness, Constr. Build. Mater. 224 (2019) 206–213, https://doi.org/10.1016/j.conbuildmat.2019.07.063.
[71] R. Yu, P. Spiesz, H.J.H. Brouwers, Development of Ultra-High Performance Fibre Reinforced Concrete (UHPFRC): towards an efficient utilization of binders and fibres, Constr. Build. Mater. 79 (2015) 273–282, https://doi.org/10.1016/j.conbuildmat.2015.01.050.
[72] H. Dehghanpour, S. Subasi, S. Guntepe, M. Emiroglu, M. Marasli, Investigation of fracture mechanics, physical and dynamic properties of UHPCs containing PVA, glass and steel fibers, Constr. Build. Mater. 328 (2022), https://doi.org/10.1016/j.conbuildmat.2022.127079.
[73] W. Li, J. Xiao, Z. Sun, S. Kawashima, S.P. Shah, Interfacial transition zones in recycled aggregate concrete with different mixing approaches, Constr. Build. Mater. 35 (2012) 1045–1055, https://doi.org/10.1016/j.conbuildmat.2012.06.022.
[74] International Organization for Standardization, EN ISO 14040:2006+A1 - Environmental Management - Life Cycle Assessment - Principles and Framework, 2020.
[75] International Organization for Standardization, EN ISO 14044:2006+A2 - Environmental Management - Life Cycle Assessment - Requirements and Guidelines, 2020.
[76] S. Marinković, I. Josa, S. Braymand, N. Tošić, Sustainability assessment of recycled aggregate concrete structures: a critical view on the current state-of-knowledge and practice, Struct. Concr. 24 (2023) 1956–1979, https://doi.org/10.1002/suco.202201245.
[77] S. Lotfi, P. Rem, Recycling of end of life concrete fines into hardened cement and clean sand, J. Environ. Protect. 7 (2016) 934–950, https://doi.org/10.4236/jep.2016.76083.
[78] S. Lotfi, P. Rem, J. Deja, R. Mróz, An experimental study on the relation between input variables and output quality of a new concrete recycling process, Constr. Build. Mater. 137 (2017) 128–140, https://doi.org/10.1016/j.conbuildmat.2017.01.085.
[79] S. Lotfi, M. Eggimann, E. Wagner, R. Mróz, J. Deja, Performance of recycled aggregate concrete based on a new concrete recycling technology, Constr. Build. Mater. 95 (2015) 243–256, https://doi.org/10.1016/j.conbuildmat.2015.07.021.
[80] D. di Summa, E. Camacho, L. Ferrara, N. De Belie, Thoroughgoing sustainability indices to support the development of a forward-looking market for innovative construction materials, Mater. Struct. 58 (2025) 12, https://doi.org/10.1617/s11527-024-02503-x.